Journal of Power Sources 195 (2010) 7880–7903

Contents lists available at ScienceDirect

Journal of Power Sources

journal homepage: www.elsevier.com/locate/jpowsour

Review

Carbon materials for electrochemical capacitors

Michio Inagaki [a,*], Hidetaka Konno [a], Osamu Tanaike [b]

[a] Professor Emeritus of Hokkaido University, Sapporo 060-8628, Japan
[b] National Institute of Advanced Industrial Science and Technology, Onogawa, Tsukuba 305-8569, Japan

ARTICLE INFO

Article history:
Received 24 April 2010
Received in revised form 11 June 2010
Accepted 11 June 2010
Available online 22 June 2010

Keywords:
Electric double-layer capacitor
Asymmetrical capacitor
Carbon electrode
Micropores
Mesopores

ABSTRACT

The carbon materials used for electrochemical capacitors were reviewed and discussed the contribution of the surfaces owing to micropores and other larger pores to the capacitance and rate performance of the electric double-layer capacitors. The necessity to have an internationally accepted specification for the measurement of capacitor performance was emphasized.

Contents

* Corresponding author. Tel.: +81 52 773 8016; fax: +81 52 773 8016.
E-mail address: im-ii@xj.commufa.jp (M. Inagaki).

0378-7753/$ – see front matter © 2010 Elsevier B.V. All rights reserved.
doi:10.1016/j.jpowsour.2010.06.036

1. Introduction

1.1. Capacitors and batteries

Carbon materials have played important roles for generation and storage of energy in different forms, such as charcoals for heat source since prehistoric age, cokes for melting and reducing natural ores for production of various metals, graphite moderators of atomic reactors for power plant and graphite anodes for lithium ion rechargeable batteries. President Obama of the United States of America started the policy so-called Green New Deal program to create new industries and to improve unemployment problems. Principal subject of his program is based on the development of renewable energies, that is, natural energy resources such as wind power, solar energy and geothermal energy. In the equipments to convert these natural energies to usable energy, mainly electric energy, carbon materials are playing an important role. For the production of silicon wafers for the solar cells high-density isotropic graphite and carbon/carbon composites are fundamental materials, and for the wind mills carbon fiber-reinforced composite is an important structural material to construct large-sized blades to get high efficiency. To store the electric energy generated by these natural energies, most of which fluctuate by their nature, lithium ion batteries (LIBs) and electrochemical capacitors are absolutely necessary devices, both of which utilize carbon materials as electrodes.

Electric energy storage in electrochemical capacitors occurs due to the formation of electric double-layer (EDL) on the surfaces of both negative and positive electrodes and to some surface oxidation/reduction. The capacitance due to the former is called electric double-layer capacitance and that due to the latter called pseudo-capacitance. If the former is the principal mechanism for the electric energy storage, the capacitors are called electric double-layer capacitors (EDLCs). Since porous carbons used often for the electrodes have some amount of oxygen- and/or nitrogen-containing functional groups on their surfaces, there is more or less a contribution of pseudo-capacitance to the observed capacitance, and so electrochemical capacitor is called “supercapacitor” or “ultracapacitor”. However, these terms are not employed in the present review. The capacitors which are consisted of different mechanisms in negative and positive electrode, for example, intercalation/deintercalation of lithium ions into the negative electrode material and adsorption/desorption of electrolyte ions (formation/disappearance of EDL) on the surface of the positive electrode material, are called hybrid capacitors.

The EDLCs are superior to LIBs because of (1) high power density (discharge at high current density), (2) short time needed for full charging, (3) long cycle life (no chemical reactions), (4) high coulombic efficiency (high reversibility), and (5) environmental friendliness (no heavy metals used), even though their energy density is lower than LIBs. In addition, the positive electrode of LIB requires certain amounts of cobalt ions, which is one of the rare metals, whereas carbon is inexhaustible. Differences between LIB and EDLC are originated from their storage mechanisms of electricity: faradaic intercalation/deintercalation reactions of lithium ions on both electrodes, positive electrode of $LiMO_2$ (M: Co, Ni, Mn, etc.) and negative electrode of graphite in LIB, but physical adsorption/desorption of electrolyte ions on both electrodes in EDLC. As a consequence, relatively high power density can be obtained, but energy density is relatively low, but charge/discharge rate and efficiency can be high in EDLCs. The capacitance of EDLCs is proportional to the effective surface area of electrode and a dielectric constant, and is inversely proportional to the thickness of EDL. The surface area of the electrodes is a crucial factor to increase capacitance, so that activated carbons with a large surface area are employed as electrodes, in addition to fairly good electric conductivity, electrochemical inertness, and lightweight properties of carbon materials. A number of reviews and articles on carbon materials related to EDLCs have been published [1–7].

On the basis of advantages described above, EDLCs using activated carbons are now set in various electronic devices and instruments, such as the backup power sources in the copy machines, the power boosters for forklifts, cranes and heavy-construction-equipments, and the street lamps and signals in combination with solar panels. The EDLCs have been used for hybrid buses and trucks, but installation to electric vehicle driveline as a main power source is thought to be difficult because of their low energy density, but there are still many efforts to get high energy density.

1.2. Cell construction of electrochemical capacitors

Information on the basic configurations of EDLC and the different types of commercial EDLC is available through various media. For fundamental studies it is unnecessary to be concerned too much about actual device structure. In this section the techniques and materials for the studies on EDLC is briefly summarized.

1.2.1. Electrolyte solution

Most of the commercial EDLCs use non-aqueous electrolyte solutions to achieve high terminal voltage, V, because the capacitor energy, E, and the maximum power, P_{max}, are given by

$$E = \frac{CV^2}{2} \text{ and } P_{max} = \frac{V^2}{4R},$$

where C is the cell capacitance in F and R is the internal resistance in Ω. The EDLCs using non-aqueous electrolyte solutions dominate the market for capacitors focusing on energy storage, but those using aqueous electrolyte solutions are also marketed. Aqueous solutions are potentially beneficial to large installations for storage of surplus power and unsteady electricity generated by natural energy resources, because of low cost, high safety, long lifetime and low internal resistance. Representative electrolytes and solvents (with abbreviations) are listed in Table 1, where some properties are also indicated [8].

In EDLCs, the sizes of cation and anion of the electrolyte are important factors in relation to the surface area, effective for the adsorption of the ions, of the electrode carbons. In the case

Table 1
Electrolytes and solvents used often.

Electrolytes	Ion size (nm)	
	Cation	Anion
Organic electrolytes		
$(C_2H_5)_4N{\cdot}BF_4$ ($TEA^+BF_4^-$)	0.686	0.458
$(C_2H_5)_3(CH_3)N{\cdot}BF_4$ ($TEMA^+BF_4^-$)	0.654	0.458
$(C_2H_5)_4P{\cdot}BF_4$ ($TEP^+BF_4^-$)		0.458
$(C_4H_9)_4N{\cdot}BF_4$ ($TBA^+BF_4^-$)	0.830	0.458
$(C_6H_{13})_4N{\cdot}BF_4$ ($THA^+BF_4^-$)	0.96	0.458
$(C_2H_5)_4N{\cdot}CF_3SO_3$	0.686	0.540
$(C_2H_5)_4N{\cdot}(CF_3SO_2)_2N$ (TEA^+TFSI^-)	0.68	0.650
Inorganic electrolytes		
H_2SO_4		0.533
KOH	0.26[a]	
Na_2SO_4	0.36[a]	0.533
NaCl	0.36[a]	
$Li{\cdot}PF_6$	0.152[b]	0.508
$Li{\cdot}ClO_4$	0.152[b]	0.474

Solvents	Melting point (°C)	Viscosity ($Pa\,s^{-1}$)	Dielectric constant, ε
Acetonitrile (AN)	−43.8	0.369	36.64
γ-Butyrolactone (GBL)	−43.3	1.72	39.0
Dimethyl ketone (DMK)	−94.8	0.306	21.01
Propylene carbonate (PC)	−48.8	2.513	66.14
Water			

[a] Stokes diameter of hydrated ions.
[b] The diameter in PC, depending strongly on the solvent used.

of non-aqueous electrolyte solutions numerous combinations of electrolytes, both organic and inorganic, with solvents are possible. The solvent itself also affects the capacitance [9,10] and certain combination is not always optimum for all carbon materials. When the electrolytes containing lithium ions was used in EDLC, the intercalation of Li^+ ions was pointed out to occur together with its adsorption onto the surface of carbon electrode [11] and also used in hybrid capacitors, as will be described later (Section 3.2). In addition to the electrolytes listed in Table 1, ionic liquids, consisting of cation of either 1-ethyl-3-methyl-imidazolium (EMI^+) or N-butyl-N-methylpyrrolidinium (PyR_{14}^+) with anion of bis(trifluoromethane-sulfonyl)imide ($TFSI^-$) [12,13] and polymer gels, such as polyethylene oxide (PEO), polymethyl methacrylate (PMMA) and polyacrylonitrile (PAN) [14,15], were proposed to be solvent-free electrolytes because they can give a large potential window but a high viscosity.

Various aqueous electrolyte solutions are commonly employed, *e.g.*, sulfuric acid, sodium sulfate and potassium hydroxide for acidic, neutral and alkaline solutions, respectively. Potassium sulfate and sodium hydroxide are also used but chloride salts are not very common probably due to specific adsorption and reducible nature of chloride ion. One of the selection criteria is the sizes of hydrated ions, although their reliable values are not yet known. Scales of ionic effective dimensions in water were estimated to be $0.362\,nm < Cs^+ < K^+ < Na^+ < Li^+ < 0.421\,nm$ and $0.362\,nm < NO_3^- < Cl^- < F^- < Br^- < 0.421\,nm$ [16]. The cation dimensions are expected to be slightly different from Stokes diameters shown in Table 1. The size of hydrated SO_4^{2-} in Table 1 is calculated one [17]. Aqueous solutions must be deaerated before and during electrochemical measurements to eliminate dissolved oxygen.

1.2.2. Test cell

For fundamental studies on the performance of single electrode, conventional three-electrode electrolytic cells are suitable, composing of working, counter and reference electrodes. In acidic aqueous solutions, a collector of working electrode should be titanium, the counter electrode is platinum or carbon, and the reference electrode is a saturated calomel electrode (SCE) or a silver/silver chloride electrode (Ag/AgCl). In neutral aqueous solutions, basically the same configuration is used but nickel can be used for a collector and the counter electrode. In alkaline aqueous solutions, a mercury/mercury oxide electrode (Hg/HgO) is used as the reference electrode. For non-aqueous electrolyte solutions case-by-case approach is required depending on the composition of electrolyte [18]. Aluminum foil is usually used for the current collector in commercially available non-aqueous capacitor, and usable also for laboratory test in typical non-aqueous electrolytes. If the test is carried out in wider potential range, other metals such as platinum are better for the test cell. However, platinum electrodes cannot be used in non-aqueous solutions containing Li^+ ions, in which nickel or copper should be used like lithium ion battery. The popular reference electrode is silver (Ag/Ag^+), and Li (Li/Li^+) is also used. Carbon is more versatile material as the counter electrode. Corresponding references should be consulted to setup experimental systems for non-aqueous solutions. Choices of the reference electrode and the counter-collector metals may be made by availability, stability in a cell, cost and so on.

In order to fabricate working electrode, active materials, *e.g.*, activated carbons (ACs), are usually mixed with a conductive agent, *e.g.*, acetylene black and Ketjen black, and a binder, *e.g.*, poly(tetrafluoroethylene) (PTFE) and poly(vinylidene fluoride) (PVDF), followed by rolling to film or forming a tablet using a compression molding press, and then by pressing onto a collector mesh or foil. Electrode thickness is a few tens micrometers to sub-millimeters depending on the active materials. The mass of active materials in the electrode must be known and preferably the electrode volume should be measured.

For evaluation of the cell performance similar to actual capacitor, two-electrode cells are recommended. This system is essential to estimate the energy density, the power density, and the cycle life of the cell. Normally two same working electrodes are set across a separator, and the potential difference between the two is monitored and controlled. In the case of perfectly symmetric two-electrode cell including sizes and charge numbers of the solvated cation and anion, the cell capacitance in $F\,g^{-1}$ is 1/4 of the single electrode capacitance measured in a three-electrode cell, theoretically. Note that the capacitance must be based on the sum of active materials in two electrodes. The capacitance values in

considerable number of literatures are indistinctive whether they are the cell capacitances or the capacitances for single electrode. It should be good to know that the capacitance of single electrode measured in a two-electrode cell does not coincide with that in a three-electrode cell because of various factors, such as the difference in sizes between the solvated cation and anion, the different potential changes of positive and negative electrodes during charge/discharge measurements, and others. Discrepancy becomes more pronounced when pseudo-capacitance is developed, because the pseudo-capacitances of negative and positive electrodes are usually very different, as will be discussed later. In the present review, the electrode, on which EDL is formed by cation adsorption, is called negative electrode and that by anion adsorption is positive electrode.

1.2.3. Electrochemical measurements

In the case of three-electrode cell, the electrode performance is evaluated by cyclic voltammetry (CV), galvanostatic chronopotentiometry (GCP), and electrochemical impedance spectroscopy (EIS). When the capacitance is simply originated from EDL, CV curves is rectangular and the capacitance is estimated from the current density at the middle point of the potential range measured, I, and the potential scan rate, r, that is, $C = I/r$. The potential range, ΔV, is depending on the electrolyte solution. When the pseudo-capacitance is added, the point of the potential for capacitance calculation should be chosen case-by-case carefully because the CV curve is not always rectangular. With increasing r, CV curves become distorted and even asymmetric. This is marked if the pseudo-capacitance is added. Accordingly, the total electric charge calculated by integrating a CV curve, Q, is often used, that is, $C = Q/(2\Delta V)$. Generally, the value of C decreases with increasing r, so that the value of r should be sufficiently low to elicit high performance. The value of Q is obtained also from a current decay curve by potentiostatic polarization. Again when the capacitance is simply originated from EDL, the potential of chronopotentiograms, V, changes linearly with time, t, at constant current density, I. Then the capacitance is given by the slope of linear relationship, dV/dt, that is, $C = I/(dV/dt)$. Similar to CV, when other factors than EDL contribute to the capacitance, the chronopotentiogram deviates from the linear relationship. It leads to arbitrariness in determining slope, so that the capacitance is usually given by $C = I \times t_T/\Delta V$, where t_T is the total time for either positive or negative process and ΔV is a potential difference after correcting an IR drop which is estimated from the initial potential jump of chronopotentiogram. Here, GCP should not be confused with charge/discharge measurements in the case of three-electrode cell, because each one slope usually includes both adsorption (charge) and desorption (discharge) processes because anion is adsorbed at more than the open-circuit voltage (OCV) and cation is adsorbed at less than the OCV in each slopes. With utilizing this, capacitances of anion and cation are often separately calculated when potential ranges of the slope are selected for calculation. For capacitor electrodes, EIS is normally carried out at the open-circuit potential by applying small amplitude of alternative potential (*e.g.*, ±5 to ±10 mV) over a wide range of frequency, f (*e.g.*, 1 mHz to 1 MHz). It provides impedance, $|Z|$, against f, and the capacitance is given by $C = 1/(2\pi f|Z|)$ using a linear portion of $\log|Z|$ *vs.* $\log f$ curve, which is known as a Bode plot. Obviously, capacitance is depending on the frequency. Alternatively, a charge-transfer resistance is given from the diameter of a semicircle in a Nyquist diagram, where the imaginary part of impedance, $Z(f)''$, is plotted against the real part of impedance, $Z(f)'$. However, numerical values of the resistance by a Nyquist diagram are not precise because perfect semicircles are not obtained usually.

Galvanostatic charge/discharge (GCD) measurements are achieved with two-electrode cells. The value of C is obtained in the same way as GCP, but it is for the full cell. In this case, for setting ΔV in non-aqueous systems, attention to the collector and counter electrode materials has to be given also, not just electrolytes and solvents, since sometimes the electrode materials are damaged by high potentials. It is recommended to carry out both three-electrode cell and two-electrode cell measurements on the same electrode material.

The capacitance per volume (C_v, *e.g.*, F m^{-3}) is practically important index of performance of the active material, but it is not so easy to estimate accurately for laboratory scale electrodes. Alternatively the capacitance per mass (C_g, *e.g.*, F g^{-1}) is used to show the performance of the active material. A large number of reported data employ the latter, though the values should be carefully evaluated for utility application because the bulk density affects to the power and energy densities of practical capacitors. Considerable number of data are reported in the capacitance per area (*e.g.*, F m^{-2}), but either one of the above two data (C_v and C_g) or the mass of electrode should be presented together.

1.3. Construction of the present review

Recent development in science and engineering on carbon materials made us possible to prepare porous carbons, not only microporous but also mesoporous carbons in different structures, textures and morphologies via various processes. Many of porous carbons developed recently cannot be classified into activated carbons, mainly because no activation process is included. Purposes of the present review are to summarize the experimental results published in various journals by focusing on the carbon materials used in electrochemical capacitors, EDLCs and hybrid capacitors, and to present some insight on carbon materials in capacitors, which may give certain information for their designing. In Chapter 2, carbon materials tested for the electrodes of electrochemical capacitors, mostly EDLCs are reviewed by paying attentions on their pore characteristics and EDLC performance. Different processes to form porous carbon materials and their characteristics are extensively reviewed in the article reported previously [19]. The addition of pseudo-capacitance due to functional groups containing oxygen and nitrogen, boron-doping and dispersion of metal particles in carbon electrode are also reviewed. In Chapter 3, new strategies for constructing electrochemical capacitors, asymmetric combinations of electrode materials for positive and negative electrodes are reviewed, including hybrid capacitors. In Chapter 4, discussion was presented on the roles of carbon materials as EDLC electrodes, demonstrating that micropores and mesopores contribute to EDLC performance differently. Importance to have international specification for the measurements of capacitive performance, capacitance and rate dependence, is emphasized.

2. Carbon materials tested as electrodes

2.1. Overview of carbon materials for capacitor

In this chapter, carbon materials tested for the electrodes of electrochemical capacitors, mostly EDLC, are reviewed by paying attentions on their pore characteristics and EDLC performance. In Table 2, carbon materials tested are summarized by describing briefly on raw materials, preparation method, a type of the cell used for capacitive performance measurements including electrolyte solution and evaluation method, and capacitance values, with some remarks.

The carbon materials were classified based on their features, such as activated carbon, templated porous carbon, nitrogen-containing carbon, and others. The materials put into plural categories were sorted by authors' judgment. Due to limitations of space, descriptions were kept to the minimum, for example, only

Table 2
Published data on the capacitive performance of carbon materials (excluding carbon nanofibers and nanotubes).

Material and method	Cell and evaluation method	Capacitance	Remarks [Ref.]
Activated carbon			
GC (air ox)	3E (3 m H_2SO_4) EIS	85–115 F mL^{-1}	Increase with oxidation time [24]
PFR (KOH ac)	2E (1 m H_2SO_4) CV	90–105 F g^{-1}	Increase with amount of KOH [25]
MP (KOH ac)	2E (1 m H_2SO_4) CV	130 F g^{-1}	Increase with amount of KOH [26]
PVDC (ht)	2E (30% H_2SO_4) CVC-GD	64 F g^{-1}	Max. at 700 °C, S_{BET} = 700 m^2 g^{-1}, no ac [36]
pitch, PFR, coconut (*nd*)	2E (1 m H_2SO_4, 1 m $LiClO_4$/PC) GCD	Fig. 1	Effect of pore size [17]
BM (steam or CO_2 ac)	2E (*nd* $TEABF_4$/PC) CVC-GD	17–33 F g^{-1}	Morphological effect [27]
c-AC (CO_2 ac)	2E (1 m $TEMABF_4$/PC) GCD	52 F g^{-1}	Increase by further ac [22]
Coal (KOH ac)	3E (1 m $LiClO_4$/PC) GCP	220 F g^{-1}	Max. at 700 °C [28]
Coal, PDC (KOH ac)	2E (1 m H_2SO_4) EIS, CV, GCD	200–320 F g^{-1}	Best performance with MP [29]
WC (CO_2 ac)	2E (1 m H_2SO_4) GCP	127–184 F g^{-1}	S_{BET} = 660–920 m^2 g^{-1} [30]
PVDF (KOH ac)	2E (1.2 m $TEABF_4$/PC) GCD, CV	39 F g^{-1}, 23 F mL^{-1}	Size effect of pore and solvated ion [31]
BM (ht)	2E (1 m H_2SO_4) CV, GCD	198 F g^{-1}	190 F g^{-1} after 6000 cycle [37]
BM, Polymers (ht, ac)	3E (7m H_2SO_4, KOH) CV	279 F g^{-1}, 267 F g^{-1}	Performance at room temp and −40 °C [33]
PDC (KOH ac)	2E (2 m H_2SO_4) GCD	400 F g^{-1}	Structural change of pores [34]
BM (steam ht)	3E (1 m H_2SO_4) GCP	280 F g^{-1}	Simultaneous ht and ac, surface area affected by ht rate, retention more than 90% at 1 A g^{-1} [38,39]
c-AC (steam ac)	2E (1.2 m $TEMABF_4$/AN) CV	60 F g^{-1}	Increase by further ac [23]
Activated carbon fiber			
IP (steam ac)	2E (1 m KCl) CVC-SCD	27–29 F g^{-1}	Effectiveness of hot briquetting before ht and ac [44]
pitch, PAN (*nd*)	2E (1 m H_2SO_4, $LiClO_4$/PC) GCD	Fig. 1	Effect of pore size [17]
MP (milled, KOH ac)	2E (*nd* $TEABF_4$/PC) CVC-GD	33–46 F g^{-1}	Morphological effect [27]
PFR (steam ht and ac, NiAA added)	3E (1 m $TEABF_4$ or $LiClO_4$/PC) GCP		Micro/mesoporous, effect of V_{meso} [41]
PFR (steam ht and ac, NiAA added)	3E (1 m $LiClO_4$/PC) GCP	Figs. 2 and 3	Micro/mesoporous [42]
IP, MP (milled, KOH ac)	2E (1 m $TEABF_4$/PC) GCD	20–46 F g^{-1}	Increase with amount of KOH [31]
Silk fibroin (ht, steam or KOH ac)	2E (1 m $TEABF_4$/PC) GD, CV	50 F g^{-1}	S_{BET} = 2600–3100 m^2 g^{-1}, V_{micro} ~ 100%, N/C < 0.02 [43]
Exfoliated carbon fiber			
MP (ht, HNO_3 ei-te)	3E (18 m H_2SO_4) CV, GCP	555 F g^{-1}	High C_g due to intercalation [57]
MP (ht, HNO_3 or H_2SO_4 ei-te)	3E (1 m H_2SO_4) CV	Fig. 4a	Increase with air ox, S_{BET} < 500 m^2 g^{-1} [56]
MP (ht, HNO_3 ei-te)	3E (1–18 m H_2SO_4) CV	1.35 F m^{-2} (per S_{BET})	Fig. 4b), high C_g due to intercalation [58]
Templated porous carbon			
FA (MSM silica, ht)	2E (2 m H_2SO_4) CV, GCD	200 F g^{-1}	Mesoporous [68]
FA (SBA-16 silica, ht)	2E (1 m H_2SO_4, 6 m KOH, 1 m $TEABF_4$/AN) CV, GCD	199, 205, 113 F g^{-1}, respectively	Mesoporous (max. 2.8 nm), good cyclability [69]
Pro, Suc (MCM-48 and SBA-15 silicas, ht)	2E (1 m H_2SO_4, 6 m KOH, 1 m $TEABF_4$/AN) CV, GCD	206, 184, 115 F g^{-1}, respectively	Best with Suc and MCM-48 [70]
Pro, Suc, Pitch (MCM-48, SBA-15 and MSU-1 silicas, ht)	3E (1 m H_2SO_4, 1 or 1.4m $TEABF_4$/AN) CV, GCP	202 F g^{-1} (aqueous) 115 F g^{-1} (non-aqueous)	Linear relationship between C_g and V_{micro} best with Suc and MCM-48 [71]
FA, TMB (6 HMS silicas, ht)	2E (2 m H_2SO_4, 6 m KOH) GCD	187, 162 F g^{-1}	Larger in the acid solution, mesoporous [74]
Suc, FA (MCM-48 and SBA-15 silicas, ht)	3E (30% KOH) CV	206 F g^{-1} at 5 mV s^{-1} 181 F g^{-1} at 50 mV s^{-1}	Mesoporous, best with FA and SBA-15, smaller than Maxsorb but better rate capability [72]
HPC, PET, PVA (MgO, ht)	3E (1 m H_2SO_4) CV, GCP	251 F g^{-1} at 20 mA g^{-1}	84% retention at 1 A g^{-1}, best with PVA [77]
FA (5 HMS, MSU and SBA silicas, ht)	2E (2 m H_2SO_4, 6 m KOH, 1 m $TEABF_4$/AN) GCD	200–220 F g^{-1} (aqueous) <100 F g^{-1} (non-aqueous)	25 Mesoporous carbons, no better than AC, denying effect of mesopores [73]
PVA (MgO, ht)	2E (2 m H_2SO_4, 1 m $TEABF_4$/AN) CV, GCD	Fig. 6	Mesoporous, good rate performance 1 → 10 A m^{-2} 85% retention [80]
PFR ($Ni(OH)_2$, ht)	3E (6 m KOH) CV	*nd*	20 → 100 mV s^{-1} 90% retention [81]
Acetylene (zeolite, CVD)	3E (1 m $TEABF_4$/PC) CV, GCP	Fig. 5	Good rate performance [62]
Acetonitrile or ethylene (zeolite Y, CVD)	2E (*nd* $TEABF_4$/AN) GCD due to large S_{BET} and V_T [63]	146 F g^{-1}	Good rate performance, N = 4.4–7.2 at% but mainly C_g

Table 2 (*Continued*)

Material and method	Cell and evaluation method	Capacitance	Remarks [Ref.]
FA and acetonitrile	2E (1.5 m $TEABF_4$/AN) GCD	160 F g^{-1}	No ac, at 0.25 A g^{-1}, retention of ca. 96% at 2 A g^{-1}
(zeolite 13X, cvd, KOH ac)		159 F g^{-1}	With ac, ~100% retention up to 2 A g^{-1} [64]
PTFE-derived carbon			
PTFE (Li defl)	3E (1 m H_2SO_4) GPC	199 F g^{-1}	Larger than ACF of similar S_{BET} [82]
PTFE (Li-naphthalenide defl)	3E (1 m $LiClO_4$/PC) GCP	123 F g^{-1}	Better rate performance than ACF [83]
PTFE (K defl)	3E (1 m H_2SO_4) GCP	229–237 F g^{-1}	Mesoporous, S_{BET} = 999–1516 m^2 g^{-1} [84]
Carbide-derived carbon			
TiC, α-SiC, Mo_2C, Al_4C_3, B_4C (chlo)	3E (1 m $TEMABF_4$/AN) CV	120 F g^{-1}	Largest C_g with Mo_2C, DFT dia. ~4 nm
	62 F mL^{-1}	Largest C_v with TiC, DFT dia. ~0.8 nm [89]	
TiC (chlo)	2E (1 m $TEMABF_4$/AN, GBL, DMK or PC) CV, GCD, EIS	102–106 F g^{-1}	Asymmetric cell: positive 1 nm, negative 1–3 nm in dia., Similar C_g except for PC [9]
B_4C, Ti_2AlC (chlo)	2E (1 m H_2SO_4) CV	175 F g^{-1}	Best with Ti_2AlC, DFT dia. peak 1 and 3 nm [92]
TiC, ZrC (chlo)	2E (1 m H_2SO_4) CV	190 F g^{-1} and 110 F mL^{-1}	With ZrC, S_{BET} ~1300 m^2 g^{-1}, both DFT dia. 0.8–1 nm
	150 F g^{-1} and 140 F mL^{-1}	With TiC, S_{BET} ~1600 m^2 g^{-1} [88]	
TiC (chlo)	2E (1.5 m $TEABF_4$/AN) CV, GCD	143 F g^{-1}	Best with S_{BET} ~1270 m^2 g^{-1}, DFT dia. 0.73 nm [90]
B_4C (HCl)	3E (6 m KOH) CV	177 F g^{-1}	Good retention, 86% for 2 → 50 mV s^{-1} [93]
Carbon aerogel			
R-F aerogel (ht)	2E (30% H_2SO_4) CVC, CRD	171 F g^{-1}	Counter electrode: graphite, S_{BET} = 560 m^2 g^{-1} [94]
R-F xerogel (ht, CO_2 ac)	3E (30% H_2SO_4) CV	185 F g^{-1}	Best at 750 °C ht without ac, S_{BET} = 795 m^2 g^{-1} [97]
R-F aerogel (ht, CO_2 ac)	2E (0.8m $TEABF_4$/PC) CV, GCD	108 F g^{-1}	Improved by surfactant treatment, V_{meso} ~ V_{micro}, S_{BET} = 1340 m^2 g^{-1} [96]
R-A cryogel (ht)	3E (1 m H_2SO_4) CV	133 F g^{-1}	Best with V_{meso} 76%, V_{micro} 24%, S_{BET} = 690 m^2 g^{-1} [98]
Oxygen-containing carbon			
PAN-CF (2 m HNO_3 dip, ht)	2E (1 m H_2SO_4) CV, GCD	160 F g^{-1} (170 F g^{-1} in abstract)	Dip at 90 °C → 450 °C in N_2, carbonyl or quinone-type, V_{micro} ~ 100% [122]
PAN-ACF (O_2 ox)	2E (1 m H_2SO_4) CV, GCD	150 F g^{-1}	Best by 250 °C, 6 h, total O = 1.31 mmol g^{-1} [120]
PAN-ACF ($NaNO_3$ e-ox)	3E (0.5 m H_2SO_4) CV	152 F g^{-1}	Increase of O-functional groups by e-ox [124]
Anthracite, IP-CF, PAN-CF	3E (1 m H_2SO_4) GCP	320 F g^{-1}	Best with anthracite and KOH ac, 25 different ACs and
(KOH, NaOH, CO_2 or steam ac)	ACFs [118]		
ACF (O_2 plasma ox)	3E (0.5 m H_2SO_4) CV	110 F g^{-1}	S_{BET} = 1570 m^2 g^{-1}, correlation with quinone group
	142 F g^{-1}	S_{BET} = 2100 m^2 g^{-1} [121]	
ACF (0.1 m HNO_3, dip or e-ox) c-AC (N_2 → H_2 ht)	2E (1 m H_2SO_4, 0.5 m $LiClO_4$/PC) GCD, CV		Increasing C_g (*cf.* text) with total amount of O-functional groups, CV → Fig. 9 [123]
MP (KOH ac, ht)	2E (1 m H_2SO_4, 6 m KOH) GCD, CV	200 F g^{-1} (in KOH)	Decrease of O-functional groups by higher HTT [119]
Nitrogen-containing carbon			
Pyridine or QL (mica temp, ht)	3E (1 m H_2SO_4) CV, GCP	156 F g^{-1}	From pyridine, W_N = 9.5 mass%, S_{BET} = 83 m^2 g^{-1}
		105 F g^{-1}	From QL, W_N = 9.5 mass%, S_{BET} = 87.5 m^2 g^{-1} [135]
PAN, PVPox, and pitch blended PAN and PVPox (ht, steam ac)	2E, 3E (1 m H_2SO_4, 1 m $TEABF_4$/AN) CV, GCD, EIS	201 F g^{-1} (aqueous)	With PAN, W_N = 7.2 mass%, S_{BET} = 807 m^2 g^{-1}
		114 F g^{-1} (non-aqueous)	With PVPox, W_N = 2.6 mass%, S_{BET} = 1420 m^2 g^{-1} [137]
M-F (mica temp, ht)	3E (1 m H_2SO_4 or NaCl) CV, GCP	105 F g^{-1}	Best at 750 °C, N/C = 0.24, $S\alpha_s$ = 442 m^2 g^{-1}, V_{meso} = 0.25 mL g^{-1}, V_{micro} = 0.13 mL g^{-1} [130]
M-F (mica temp, ht)	3E (1 m KOH, 1 m $TEABF_4$/PC) CV, GCP, EIS	208 F g^{-1} (aqueous)	same material as [Hulicova05], W_N ~ 25 mass%,
		37.5 F g^{-1} (non-aqueous)	S_{CO2} ~ 260 m^2 g^{-1}, V_{micro} = 0.29 mL g^{-1} [128]
QL-pitch (SBA-15 temp, ht)	3E (1 m H_2SO_4) CV, GCP	289 F g^{-1}	Best at 750 °C, W_N = 9.4 mass%, S_{BET} = 729 m^2 g^{-1} [138]
Melamine foam (ht)	3E (1 m H_2SO_4) CV, GCP	241 F g^{-1}	Best at 800 °C, W_N = 21 mass%, non-porous [126]

Table 2 (*Continued*)

Material and method	Cell and evaluation method	Capacitance	Remarks [Ref.]
M-F (silica temp, ht)	3E (5 m H_2SO_4) GCP	211 F g^{-1}	29 nm Mesopore, W_N = 10 mass%, S_{BET} = 1330 m^2 g^{-1} [139]
Polyaniline (ht)	3E (1 m H_2SO_4) GCP	157 F g^{-1}	Best at 800 °C, N/C = 0.1, S_{BET} = 34 m^2 g^{-1} [136]
c-AC (50% HNO_3, ht, urea or melamine)	2E (1 m H_2SO_4) CV, GCP	330 F g^{-1}	Changing treatment order, best with direct melamine treatment, W_N = 5.9 mass%, S_{BET} = 1435 m^2 g^{-1} [141]
FA, acetonitrile (zeolite temp, CVD)	2E (1.5 m $TEABF_4$/AN) GCD	150–160 F g^{-1}	W_N = 5.3–6.5 mass%, S_{BET} = 1800–2700 m^2 g^{-1}
		160 F g^{-1}	KOH ac → W_N = 0.5 mass%, S_{BET} = 2860 m^2 g^{-1} [64]
PAA, TMM, PVP (MgO temp, ht)	3E (1 m H_2SO_4) CV, GCP	234 F g^{-1}	Best with PAA, W_N = 8.2 mass%, S_{BET} = 840 m^2 g^{-1}, increasing C_g/S_{BET} with W_N [140]
Boron-containing carbon			
GL-H_3BO_3 complex (ht)	3E (1 m H_2SO_4 or Na_2SO_4) CV, GCP	227 F g^{-1} (in H_2SO_4)	W_B ~ 2 mass%, S_{BET} = 1355 m^2 g^{-1}, clear redox peaks, no direct relationship between C_g and W_B [144]
Citric acid-H_3BO_3-NH_3 gel	3E (6 m KOH) CV	247 F g^{-1}	B ~ 8.4 at%, N ~ 7.1 at%, O ~ 14.7 at% by XPS,
($NiCl_2$, ht and ac)	2E (6 m KOH) GCD	268 F g^{-1}	S_{BET} = 894 m^2 g^{-1} [145]
PAA-H_3BO_3 mixture (ht)	3E (1 m H_2SO_4, Na_2SO_4 or Li_2SO_4)	305 F g^{-1} (in H_2SO_4)	W_B ~ 6–9 mass%, S_{BET} ~ 410 m^2 g^{-1}, formation of C–B–O and B–N bonds in carbon [146]
	CV, GCP	135 F g^{-1} (in neutral sol.)	

Material: c-AC = commercial activated carbon, BM = biomass, FA = furfuryl alcohol, GL = glucose, HPC = hydroxyl propyl cellulose, IP = isotropic pitch, M-F = melamine-formaldehyde, MP = mesophase pitch, NiAA = nickel(II) acetylacetonate, PAA = polyacrylamide, PAN = polyacrylonitrile, PET = poly(ethylene terephthalate), PFR = phenol-formaldehyde resin, Pro = propylene, PTFE = poly(tetrafluoroethylene), PVA = poly(vinyl alcohol), PVDC = poly(vinylidene chloride), PVP = poly(vinylpyrrolidone), PVPox = oxidized poly(4-vinylpyridine), QL = quinoline, R-A = resorcinol-acetaldehyde, R-F = resorcinol-formaldehyde, Suc = sucrose, TMB = trimethylbenzene, TMM = trimethylolmelamine, WC = wood charcoal.
Method: ac = activation, chlo = chlorination, cvd = chemical vapor deposition, defl = defluorination, ei-te = electrochemical intercalation and thermal exfoliation, e-ox = electrochemical oxidation, ht = carbonization or heat treatment under an inert atmosphere, ox = oxidation, temp = template.
Cell: 2E = two-electrode system, 3E = three-electrode system, m: mol L^{-1} (Abbreviations for electrolytes and solvents are in Table 1).
Evaluation method: CVC = constant voltage charge, CRD = constant road discharge, GCP = galvanostatic chronopotentiometry, GCD = galvanostatic charge/discharge, GD = galvanostatic discharge, SCD = short-circuited discharge, *nd*: no detailed description.

one datum of capacitance (mostly the largest one) was listed in the table, even though capacitances in different electrolytes were reported in the reference. In taking a look of this table, particular attention should be given to the following points:

(1) The capacitance values are mostly the largest one in each reference. It implies that in the case of CV, sweep rate is very low (almost always less than 5 mV s^{-1}), and in the case of GCP, current density is very low (sometimes less than a few mA g^{-1}).
(2) In the case of two-electrode cell, a considerable number of data are vague whether they are capacitances for the single electrode or the cell (*cf.* Section 1.2). Some of them may be judged from excessive values but distinct description on this crucial point lacks in no small part of the papers.
(3) In some references using plural evaluation methods, there was no clear description which method was used to estimate the capacitance values in the text.

At the present state of no internationally accepted specification for capacitance measurement, as will be discussed latter, it does not make too much sense emphasizing the capacitance values in Table 2. The particulars below are basically described in order appeared in the table without experimental details because they are shown in Table 2.

2.2. Nanoporous carbons prepared by different methods

2.2.1. Activated carbons

A number of activated carbons (ACs), either commercially available or laboratory-made, were tested as the electrode materials for EDLCs, because high surface area was thought to be a primary requirement to give high capacitance. In the literatures reporting on EDLC performance on various carbon materials reviewed below, commercial ACs were often used as reference materials.

EDLC capacitance was measured on commercial ACs having S_{BET} of 500–1700 m^2 g^{-1} in 30% KOH, which could not correlated to the total surface area determined by DFT method [20]. The author showed that the observed capacitance could be explained by the different contributions from microporous and external surfaces. Discussions differentiating the roles of micropore and mesopore, however, are not sufficiently developed except for limited number of references (*cf.* Section 4.1). Twelve commercial ACs having S_{BET} = 1150–2570 m^2 g^{-1} were tested in 30% KOH, and the capacitance did not give a clear dependence on S_{BET}: 100 F g^{-1} for AC with 2130 m^2 g^{-1} but 63 F g^{-1} for AC with 2570 m^2 g^{-1} [21]. The authors pointed out that the carbon having large pores was supposed to be suitable to high power capacitors, because of the possibility for the discharge at a high rate. Re-activation of commercial ACs was also carried out to improve EDLC performance, and reported to have a beneficial effect [22,23]. As a general tendency, increasing amount of KOH on activation increases S_{BET}, leading to higher capacitance.

To understand significance of the pore structure in electrode carbons to EDLC performance and to develop the preparation conditions of carbons for better performance, a variety of ACs were prepared from different precursors under different activation conditions [17,24–35]. From some precursors, high performance porous carbons are obtained through a simple pyrolysis without activation [36–38]. A porous carbon derived from poly(vinylidene chloride) (PVDC) at 700 °C was shown to have high C_g at different current densities of 1–100 mA cm^{-2} [36]. Carbons prepared from seaweed (sodium alginate) by carbonization at 600 °C exhibited high C_g and excellent cyclability [37]. Five porous carbon materi-

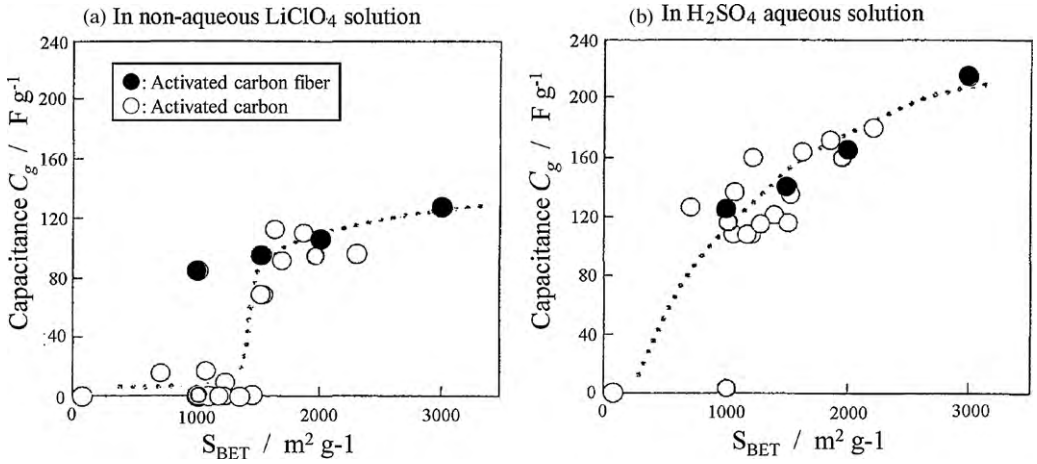

Fig. 1. Relation between capacitance C_g in non-aqueous and aqueous electrolyte solutions with BET surface area S_{BET} for various activated carbons and activated carbon fibers (courtesy of Prof. M. Endo of Shinshu Univ.) [17].

als were prepared from different precursors (peach stone, furfuryl resin, saran, and others) with or without activation [33]. The carbons having S_{BET} = 2100 and 2700 m^2 g^{-1} retained the capacitance at a low temperature as −40 °C with 10 and 25% reduction, respectively, much smaller decrease than other carbons of smaller S_{BET}. A high retention in capacitance, the ratio of the capacitance measured with the current density of 100 mA g^{-1} to that with 10 mA g^{-1} was obtained on the cypress chips carbonized in super-heated steam, which was supposed mainly due to marked development in external surface area, S_{ext} [38,39].

2.2.2. Activated carbon fibers

Activated carbon fibers (ACFs) have to be differentiated from ACs because of their pore structures: micropores are directly exposed to the surface of the fiber in ACFs but they are formed on the wall of macropores and mesopores in ACs [19]. Therefore, fast adsorption/desorption of adsorbent molecules can be expected on ACFs.

The value of C_g is plotted against S_{BET} for four ACFs together with various ACs in Fig. 1 [17]. Capacitance was not measurable in $LiClO_4$/PC electrolyte for ACs with S_{BET} < 1400 m^2 g^{-1}, although C_g in a H_2SO_4 solution was relatively high, except one AC. On the other hands, ACFs can give relatively high capacitance in both electrolytes, suggesting that the difference in pore structure between granular AC and fibrous ACF gives that in EDLC performance. EDLC performance was discussed from the relation between ion sizes of solvated electrolyte and pore size in carbon electrodes composed from AC and ACFs. Morphological effect was discussed also for milled ACFs derived from pitches, and activation was shown to be essential to get high capacitance in a non-aqueous electrolyte solution [27,40].

Mesoporosity was introduced into microporous ACFs by simultaneous carbonization and activation in steam of the novolac-type phenol resin added with Ni complex [41,42]. Addition of Ni markedly increased V_{meso} from 0.16 mL g^{-1} (without Ni) to 0.86 mL g^{-1}, leading to larger C_g [41]. In Fig. 2a–c, the total C_g calculated from overall potential-time curves in a range of 2.0–4.0 V *vs.* Li/Li$^+$ and the values of C_g calculated by dividing the curves into two ranges corresponding to cation (3.0–2.0 V) and anion (3.0–4.0 V) adsorption are plotted against S_{BET}, respectively [42]. Cation adsorption gives smaller capacitance than anion adsorption does for both ACFs (with and without Ni added), but the difference between these two ACFs is more marked in cation adsorption. The results suggest that solvated Li$^+$ ion having larger size (0.82 nm) may be less easy to be adsorbed into micropores than ClO_4^- ion having smaller size (0.52 nm) (ion sieving of micropores) and that mesopores may assist the diffusion of Li$^+$ to micropores. For the same ACFs, values of C_g measured in a range of 2.25–3.75 V are plotted against current density in Fig. 3 [42]. ACFs with relatively large amount of mesopores show good rate performance.

ACFs derived from silk fibroin had very large surface area (S_{BET} = 2600–3100 m^2 g^{-1}) and large cell capacitance, but had

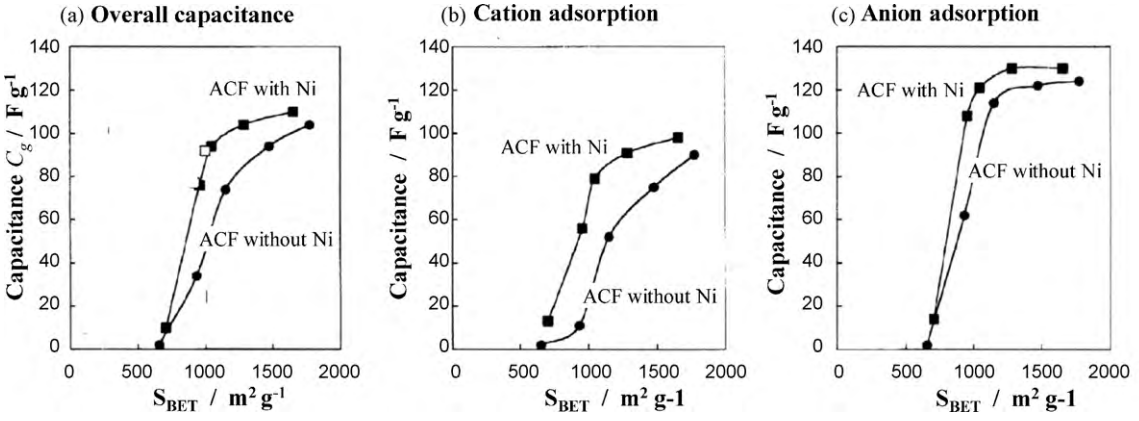

Fig. 2. Dependences of total capacitance C_g and capacitances due to cation and anion adsorption in 1 mol% $LiClO_4$/PC on BET surface area S_{BET} for activated carbon fibers prepared from phenol resin with or without Ni complex (courtesy of Prof. S Shiraishi of Gunma Univ.) [42].

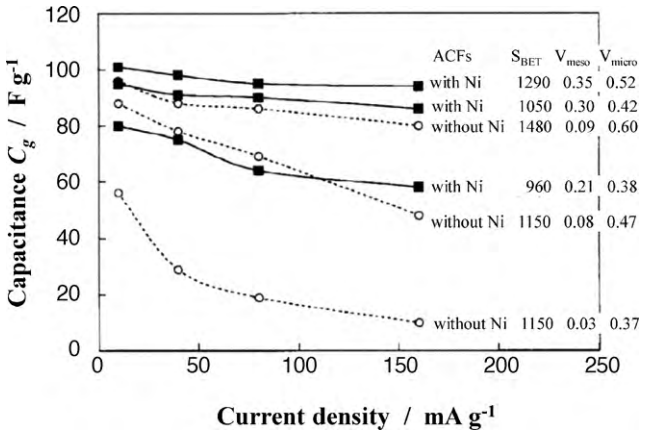

Fig. 3. Dependences of total capacitance C_g on current density for activated carbon fibers prepared from phenol resin with or without Ni complex (courtesy of Prof. S Shiraishi of Gunma Univ.) [42].

low bulk density, ρ_b (0.4–0.47 g mL^{-1}) [43]. Usually, ACF has $\rho_b \sim 0.2$ g mL^{-1} which is disadvantageous for electrodes of EDLC. Hot briquetting of isotropic-pitch fibers after stabilization was reported to increase the capacitance of the cell [44]. Electrode sheets with ρ_b = 0.36–0.81 g mL^{-1} were prepared by hot briquetting at 400 °C under a pressure up to 20 MPa, followed by carbonization and activation. With increasing ρ_b the capacitance of coin cell increased from 2.69 to 7.20 F, but C_g did not change, about 28 F g^{-1}.

In addition to ACFs commercially available, various carbon fibers (CFs), included so-called nanofibers, were activated in the laboratories and studied the effectiveness of activation process for the improvement in performance of electrochemical capacitors [45–54]. Carbon nanofibers, most of them being synthesized by catalytic CVD process, had often been called multi-walled carbon nanotubes, even in the literatures listed above. However, they are different in structure and have to be differentiated from carbon nanotubes, including single-, double- and multi-walled ones. Carbon nanofibers can be activated by conventional process using KOH and air to increase surface area.

2.2.3. Exfoliated carbon fibers

Alternative way to get high surface area on carbon fibers is their exfoliation. Morphology of fibers after exfoliation depends on the starting carbon fibers [19,55].

In Fig. 4a, C_g measured on exfoliated CFs prepared from 3000 °C-treated mesophase-pitch-based CFs is plotted against S_{BET}, together with some data on ACFs [56]. Exfoliated CFs do not have so high S_{BET} as commercial ACFs, but show relatively high C_g. In contrast to microporous ACFs, exfoliated CFs are characterized by the presence of large amounts of mesopores, which can be supposed from a marked hysteresis in adsorption/desorption isotherm of N_2 shown in Fig. 4b. By air-oxidation (activation) of exfoliated CFs, capacitance increased markedly, although S_{BET} increased slightly. With these exfoliated CFs, huge capacitance as 450–555 F g^{-1} was realized in 18 mol dm^{-3} H_2SO_4 [57,58]. Such high capacitances were supposed to come from pseudo-capacitance due to intercalation of H_2SO_4 molecules (faradaic reaction) into graphite gallery of exfoliated CFs, in addition to double-layer capacitance. Stable galvanostatic charge/discharge was confirmed for these exfoliated CFs over 7000 cycles at 500 mA g^{-1}. In the cyclic voltammogram for this electrode, no peak corresponding to redox reaction due to intercalation was observed.

2.2.4. Templated porous carbons

Template method can form both microporous and mesoporous carbons depending on templates and raw materials, and the proportion of them is possible to be changed to some extent [19].

Through the carbonization of precursors in nanochannels of various types of zeolite, microporous carbons (zeolite-templated carbon, ZTC) were prepared, of which the highest S_{BET} and total pore volume were about 4000 m^2 g^{-1} and about 1.8 mL g^{-1}, respectively [59–62]. Since the pores formed in ZTC are inherited from zeolite channels, formed micropores are homogeneous in both size and morphology, having only a small amount of mesopores. CV curves of ZTC in a non-aqueous solution showed non-rectangular patterns, which was pointed out to be due to pseudo-capacitance mainly resulted from oxygen functional groups on the carbon surface, but C_g did not correlate to oxygen content [62]. The values of C_g for various ZTCs are plotted as a function of current density in

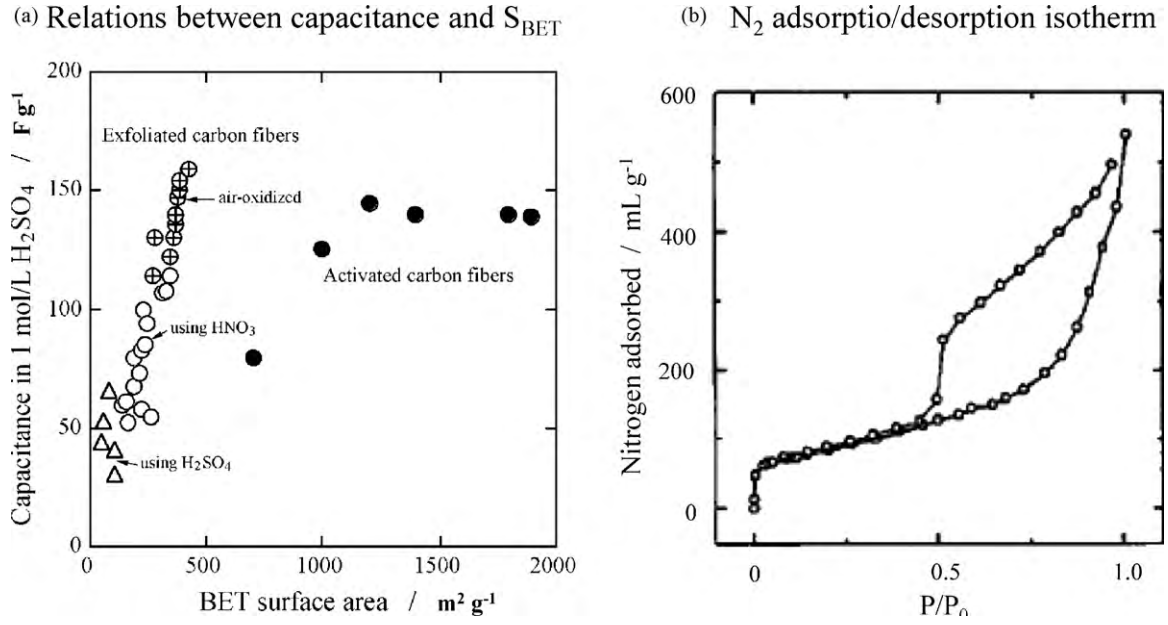

Fig. 4. Relations between capacitance C_g in 1 mol L^{-1} H_2SO_4 and BET surface area S_{BET} for exfoliated carbon fibers compared with activated carbon fibers (a) and adsorption/desorption isotherm of N_2 for an exfoliated carbon fibers (b) (courtesy of Prof. M. Toyoda of Oita Univ.).

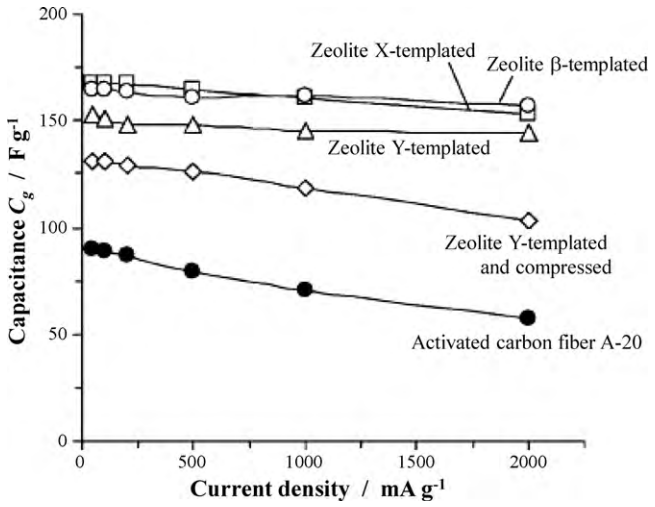

Fig. 5. Dependences of capacitance C_g on current density for zeolite-templated carbons (ZTCs) in 1 mol L^{-1} $TEABF_4$/PC (courtesy of Prof. T. Kyotani of Tohoku Univ.) [62].

Fig. 5, together with C_g for a commercial ACF. For most of the ZTCs, very good rate performance has to be pointed out, almost constant capacitance even at as high current density as 2000 mA g^{-1}, in addition to high C_g. This excellent rate performance was supposed to be due to three-dimensionally ordered micropores, giving a low ion-transfer resistance in micropores. Similar results were obtained with ZTCs prepared by using acetonitrile or ethylene with zeolite Y [63]. Another microporous ZTCs were prepared via two-step casting process using zeolite 13X template, followed by KOH activation [64]. Retention of capacitances as high as 94–100% was demonstrated up to the current density of 2 A g^{-1} for non-activated and activated ZTCs.

Mesoporous carbons were prepared using mesoporous silicas: two-dimensional hexagonal mesoporous silica (*e.g.*, SBA-15) gives the carbons having two-dimensionally ordered mesopores, and three-dimensional cubic mesoporous silica (*e.g.*, MCM-48) gives the carbons having three-dimensionally ordered mesopores [65–67]. Probably the capacitive performance of these carbons was first reported for that prepared from phenol-formaldehyde with MCM-48 implanted with aluminum [66]. However, only the difference of CV curves between silica-templated carbons and a commercial AC was demonstrated.

Using mesoporous silica, the first impregnation of furfuryl alcohol resulted in bimodal mesoporous carbons with the population maxima at 2.9 and 16 nm, but by further impregnation a unimodal one with 2.8 nm size was obtained [68]. The S_{BET} was 1540–1810 m^2 g^{-1} and more than a half of total pore volume was ascribed to mesopores. The C_g was 200 F g^{-1} at 1 mA cm^{-2} but markedly decreased with increasing current density. For similar mesoporous carbons, good cyclability and C_g retention of 77–97% after 3000 cycles at 500 mA g^{-1} were reported [69]. The two-dimensional and three-dimensional networks of mesopores were prepared from propylene or sucrose using SBA-15 and MCM-48 silica templates, respectively [70]. Three-dimensional network of mesopores in the carbons gave better performance than two-dimensional ones. Among various combinations of carbon precursors with templates, the combination of sucrose and MCM-48 showed the best performance [71]. Although a number of works pointed out the presence of mesopores as beneficial structure for EDLC, a study with 25 silica-templated carbons, having different pore structures and surface areas of 200–1560 m^2 g^{-1}, concluded that these silica-templated carbons do not show obvious advantages over ACs both in aqueous and non-aqueous solutions [73].

For mesoporous carbons formed with six silica templates and had S_{BET} = 1330–2250 m^2 g^{-1}, absence of micropores was confirmed by different techniques [74]. By coupling with a conventional activation process, micropores could be easily introduced into mesoporous carbons [75,76]. By CO_2 activation, C_g in 6 mol L^{-1} KOH by CV at a sweep rate of 2 mV s^{-1} increased from 115 F g^{-1} up to 223 F g^{-1} [76]

Mesoporous carbons were also prepared by using MgO particles as a template [77–79]. The process has some advantages for the preparation of mesoporous carbons because MgO particles can be dissolved out by a weak acid, such as citric acid, and re-used as a template precursor, and the resultant carbons have a sharp pore size distribution in mesopore regions. MgO-templated mesoporous carbons are characterized by a high percentage retention at high charge/discharge rate both in aqueous and non-aqueous solutions, as shown in Fig. 6 [77,80]. High retention in capacitance was related

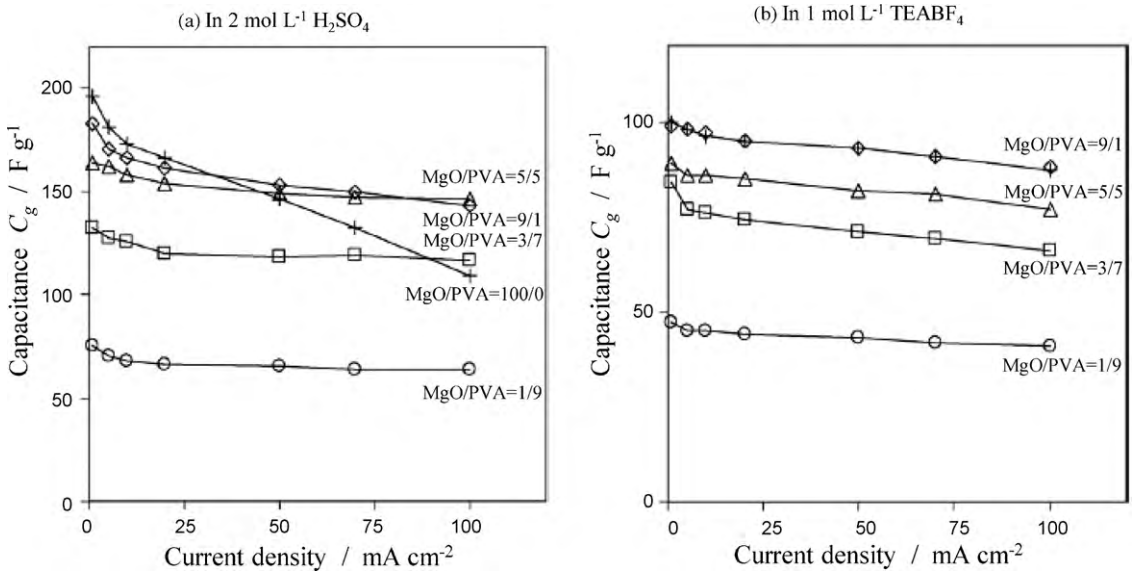

Fig. 6. Dependences of capacitance C_g in aqueous and non-aqueous electrolyte solutions on current density for MgO-templated carbons [77,80].

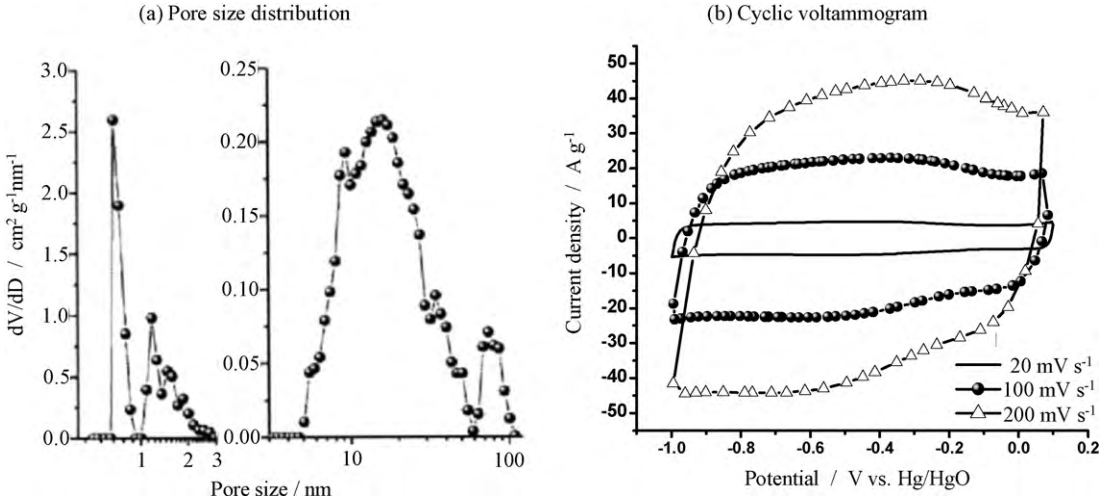

Fig. 7. Pore size distributions and cyclic voltammograms with different sweep rates for a $Ni(OH)_2$-templated carbon (courtesy of Prof. H.-M. Cheng of Chinese Academy of Science) [81].

to S_{ext} of the carbons, which consisted mainly of the mesoporous surface area [77].

Mesoporous carbons were prepared by a similar procedure to MgO-template method using $Ni(OH)_2$ [81]. The pore structure might be characterized by micropores of 1–2 nm, mesopores of 5–50 nm and macropores of 60–100 nm, as shown in Fig. 7a. As shown in Fig. 7b, CV curves are rectangular even at a high sweep rate as 100 mV s^{-1} and 90% capacitance retention is achieved in a range of 20–100 mV s^{-1}, the performance being superior to commercial ACs and silica-templated carbons.

2.2.5. Poly(tetrafluoroethylene)-derived carbons

Defluorination of poly(tetrafluoroethylene) (PTFE) by using alkali metals and in 1,2-dimethoxyethane solution of alkali metal naphthalenide at room temperature was found to give porous carbons (PTFE-derived carbons), composing from both micropores and mesopores [19].

Performance of PTFE-derived carbons as capacitor electrodes was evaluated both in aqueous and non-aqueous solutions [82–84]. Examples comparing PTFE-derived carbons to ACFs are shown in Fig. 8a and b [83,84], revealing that PTFE-derived carbon gave much higher capacitance than ACFs. Mesopores were predominant in PTFE-derived carbons, but micropores were predominant in ACFs. This difference in pore structure of these two carbon materials was supposed to be the main reason for the different dependence of capacitance on S_{BET}. By γ-ray irradiation, S_{BET} increased markedly (Fig. 8a), but it was mainly due to the increase in mesopores, so that γ-ray irradiation was not so much effective to increase capacitance and also to improve the rate performance.

2.2.6. Carbide-derived carbons

Various metal carbides were found to give highly microporous carbons through the heat treatment at a temperature from 400 to 1200 °C in a flow of Cl_2 [85]. The S_{BET} was reported to be 1000–2000 m^2 g^{-1}. Pore structure of these carbons depends

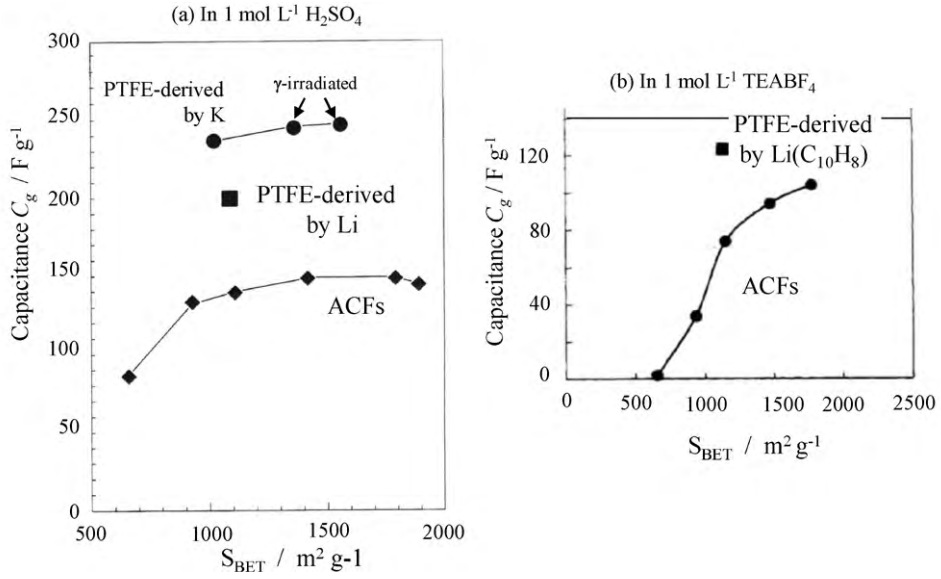

Fig. 8. Relations between capacitance C_g in aqueous and non-aqueous electrolyte solutions for PTFE-derived carbons in comparison with activated carbon fibers (ACFs) (courtesy of Prof. S Shiraishi of Gunma Univ.).

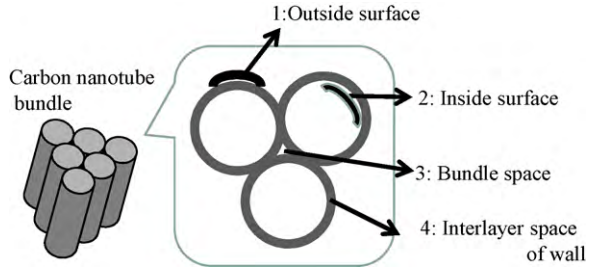

Fig. 9. Schematic illustration of the spaces in a carbon nanotube bundle for the storage of electrolyte ions.

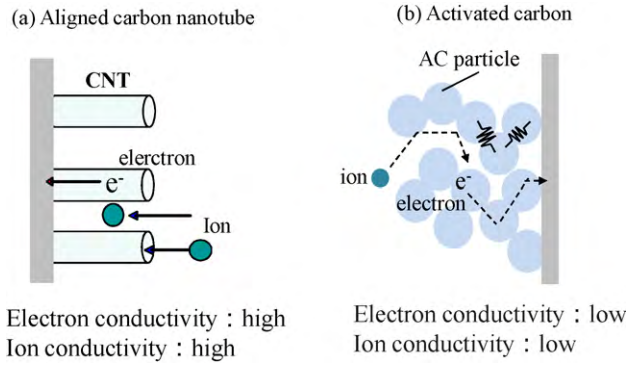

Fig. 10. Comparison on conducting paths for electron and electrolyte ion in an aligned carbon nanotubes and granular activated carbon.

strongly on the precursor carbide and heat treatment temperature (HTT). In these carbide-derived carbons, micropores are mainly formed up to about 800 °C, but mesopores become predominant above 800 °C, as a consequence, S_{BET} showing a maximum around 800 °C in most of the carbons [86–88].

By using these carbide-derived microporous carbons, EDLC behavior was studied in various non-aqueous solutions [89–91] and a H_2SO_4 solution [92], and discussed on the effects of ion sizes of electrolytes and of the organic solvents used [11,9]. For TiC-derived carbons prepared at 500–1000 °C, in which average micropore size and S_{BET} changed from 0.7 to 1.1 nm and 1000 to 1600 $m^2\,g^{-1}$, respectively, the capacitance normalized by S_{BET} was shown to increase with decreasing average pore size [90]. B_4C-derived carbons gave a good rate performance in a KOH solution, about 86% retention by the change in sweep rate from 2 to 50 $mV\,s^{-1}$ [93].

2.2.7. Carbon aerogels and xerogels

Carbon aerogels having large amounts of mesopores were prepared mostly by pyrolysis of the aerogels of resorcinol and formaldehyde [19,95]. Primary particles of carbon aerogels have usually the size of about 4–9 nm and interconnected with each other to form a network, forming interparticle mesopores.

Changes in preparation conditions of carbon aerogels gave a strong effect on capacitive performance of EDLC: the increase in resorcinol to basic catalyst (R/C) resulted in the increase in S_{BET} but a slight decrease in C_g in 30% H_2SO_4 and the solution with pH of 7.3–7.7 gave mesopore-rich carbon and consequently high C_g. In order to apply carbon aerogels to EDLC electrode, activation was shown to be necessary to develop micropores in the primary particles [96]. The CO_2 activation resulted in the development of the comparable amount of micropores to mesopores, and about twice larger capacitance in a non-aqueous solution. Surface modification of this carbon aerogel with a surfactant (sodium oleate) could give higher capacitance at higher current density, which may be due to the improvement in wettability of the carbon surface to organic electrolytes [96].

The value of C_g for a carbon xerogel increased from 112 to 171 $F\,g^{-1}$ by activation with CO_2, this change in C_g being associated with marked increase in S_{micro} from 530 to 1290 $m^2\,g^{-1}$ together with an increase in S_{meso} from 170 to 530 $m^2\,g^{-1}$ [97].

2.3. Carbon nanotubes

2.3.1. Advantages of carbon nanotubes

Carbon nanotubes (CNTs) are expected also attractive for capacitor electrode materials. Their important and promising characters for capacitor electrode materials are based on not only their large area of exposed surface and different storage spaces for electrolyte ions, but also their high electrical conductivity. Storage spaces in carbon nanotubes are illustrated in Fig. 9. Outside surface of the wall of CNTs (1 in Fig. 9) consists principally of the basal plane of graphite, so that there is no edge plane. At the edge planes, irreversible electrochemical reactions, such as electrolyte decomposition, easily occur at a high potential, which prevent from using the capacitor at high voltage. On such an ideal surface of CNTs, therefore, a large capacitance of EDL is expected to be accompanied by a wide potential window. However, most of the CNTs are known to be bundled with each other due to the van der Waals force, where only the outermost tubes in a bundle are exposed to the electrolyte and so-called bundle spaces among tubes (3 in Fig. 9) are difficult to be used for the formation of EDL. Consequently, debundling of most of the CNTs is required in order to make all the surface of tubes available for EDL formation. The inner surface of nanotubes (2 in Fig. 9) is also useful for the access of electrolyte ions if suitable openings are formed. Interlayer space in the wall of multi-walled nanotube (4 in Fig. 9) can be intercalated by an electrolyte ion such as Li^+. Therefore the intercalation might be possible also as faradaic reaction to give a pseudo-capacitance. However, it must be pointed out that excess enlargement of the interlayer spaces by intercalation will cause some degradation of the electrode which shortens the cycle life of the capacitor.

In addition, the electrode composed from aligned CNTs has some merits for the capacitive performance with a high power. In Fig. 10, the conducting paths for electrolyte ions and electrons in the aligned CNTs are schematically compared with activated carbon (AC). The electrode composed from AC particles and a binder has a large internal resistance because of both many contact points between the particles and insulating binder material (Fig. 10b). In contrast, if the CNTs are aligned on a current collector, internal resistance is reduced enough because both ion and electron conductive paths are simplified as shown in Fig. 10a. In addition, CNTs themselves usually have higher conductivity than ACs.

2.3.2. Single-walled carbon nanotubes

Capacitive performance of single-walled carbon nanotubes (SWCNTs) have been measured by using various electrolytes, from organic electrolyte [99,100] to aqueous solution [101–103] in various literatures, even though SWCNTs are strongly bundled. Most of them tend to conclude that SWCNTs have more excellent properties as electrode materials than ACs. However, it should be careful to discuss their results by using only the capacitance value, as similarly as other porous carbons mentioned above, because their synthesis methods, qualities of tubes used and evaluation methods are different from each other. The gravimetric capacitance C_g per BET surface area, *i.e.*, the ratio C_g/S_{BET}, determined on commercially available SWCNTs (HiPcoTM) was reported to be about 10^5 $F\,m^{-2}$ [2], about twice of ACs (5.5×10^4 $F\,m^{-2}$), even though C_g is much smaller than ACs. It reveals that individual nanotube potentially has a larger specific capacitance than that of ACs, but the bundle space of CNTs and the inner surface of each CNTs are not used for the formation of EDL. The surface area of SWCNTs was enhanced

by their electrochemical oxidation and the capacitance in 6 mol L^{-1} KOH solution could increase to be three times larger [103]. SWCNT synthesized by highly efficient process, so-called "super growth method" was reported to have a high S_{BET} as more than 1000 $m^2\ g^{-1}$ [104], in comparison with commercially available SWCNTs having 400–800 $m^2\ g^{-1}$. The super-grown SWCNTs could be debundled to expose more than 80% of the surface area calculated from the diameter of the tubes for the electrolyte solution, and as a consequence a large capacitance was obtained in an organic electrolyte, the larger capacitance at the higher potential [105], as shown in Fig. 11. These highly debundled high-purity SWCNTs showed a high capacitance, of which potential dependence was explained by electrochemical doping/undoping of the electrolyte ions during charge/discharge [106]. These data suggest that pure and debundled SWCNT is potentially useful as an electrode material with larger capacitance at higher voltage than typical ACs.

In order to use the inner surface of SWCNTs, the formation of some openings in the tube was tried through an oxidation process. If the inner surface of opened SWCNTs could be completely utilized for the formation of EDL, the capacitance is simply supposed to be doubled. However, the optimization of oxidation condition is very important and difficult because strong oxidation treatment of SWCNTs might deteriorate the tube quality by introducing various defects and/or making the tubes shortened by chopping, even if the specific surface area was enhanced. By the optimization of the oxidation conditions of super-grown SWCNTs for their capacitor use, S_{BET} of more than 2000 $m^2\ g^{-1}$ was achieved and the capacitor using $TEABF_4$/PC gave a high capacitive performance, 24.7 W h kg^{-1} in energy density and 98.9 kW kg^{-1} in power density [107]. However, the increase in capacitance was not in proportion to the increase of S_{BET}, suggesting further precise condition of forming the openings in the tubes for the access of the electrolyte ions.

Vertically aligned SWCNTs with high purity and density on a substrate were synthesized by CVD [108], from which SWCNT "solid" was possible to prepare through self packing of vertically aligned SWCNTs by zipping effect of liquids to draw tubes. SWCNT solid thus prepared was successfully used as electrodes without any insulating binder, of which the electrical conductivity reached 13 S cm^{-1}, more than 20 times larger than that of the conventional electrodes composed from AC with a binder, and as a consequence the capacitance was larger than AC, particularly at extremely high current density as higher than 10 A g^{-1}.

2.3.3. Double-walled and multi-walled carbon nanotubes

Compared with SWCNT, capacitor properties of double-walled carbon nanotubes (DWCNTs) have not been so frequently reported, because pure DWCNTs have been slightly difficult to be obtained. In principle, DWCNT and multi-walled carbon nanotubes (MWCNTs) have less surface area for EDL than SWCNT. The comparison between DWCNT and SWCNT, both commercially available (HiPcoTM) [109] showed that the electrochemical properties of DWCNT are quite similar to SWCNT, but the capacitance value of DWCNT does not surpass that of SWCNT, because the surface area of DWCNT cannot exceed SWCNT.

In contrast, there have been many reports on capacitive performance of MWCNTs because MWCNTs are relatively easy to be synthesized. Depending on the synthesis methods and the modification, various types of MWCNTs having various surface areas are obtained and so the capacitance values are widely distributed in both aqueous and non-aqueous electrolytes from 10 to 200 F g^{-1} [101,102,110–112]. However, they are not so surprising values in comparison with those of ACs. On the other hand, it has to be pointed out that the volumetric capacitance C_v is relatively high because the bulk density of MWCNT is high [112].

An effective improvement in capacitive performance by aligning was also reported on MWCNTs [113] and DWCNTs [114]: the CNTs were synthesized by catalytic CVD and then transferred to an aluminum current collector using a small amount of conductive cement to make them vertically aligned. The rate performance of DWCNTs and MWCNTs was quite excellent even at a high current density as 20 A g^{-1}, but the capacitance value of DWCNTs was larger than MWCNTs. Plasma-etching was applied on the aligned MWCNT to open the end cap of tubes and reported a high capacitive performance, a high cell voltage, high energy density, and high power density, of the opened and aligned carbon nanotube electrodes with a large electrochemical window in ionic liquid electrolytes [115].

MWCNTs were also reported to be used as current collecting substrates for other active materials, such as conductive polymer, because of their high conductivity [101].

2.4. Carbons containing heteroatoms

2.4.1. Oxygen-containing carbon

Carbon materials can have various functional groups on their surface, most of them being reasonably supposed to be bonded

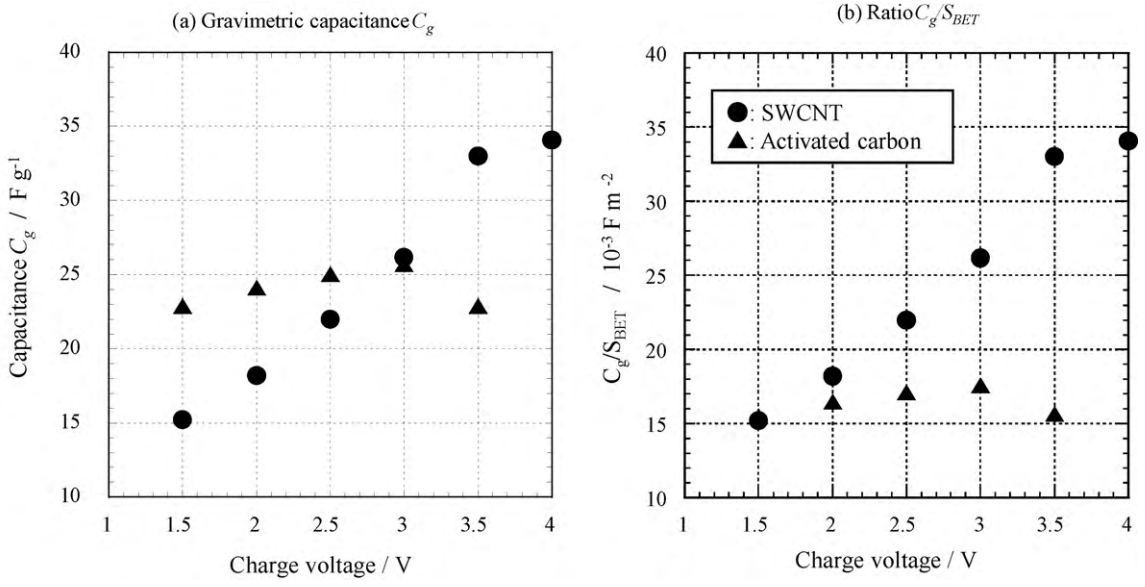

Fig. 11. Capacitance C_g and its ratio to S_{BET} for the debundled single-walled carbon nanotubes in comparison with an activated carbon [105].

with carbon atoms at the edge of hexagonal carbon layers. These functional groups contain often oxygen, such as –COOH, =CO, and others, dependent strongly on the precursors and preparation conditions of the carbon material. Some of these functional groups were understood to be acidic and electrochemically active, and to contribute to the capacitance of EDLCs, which is called pseudo-capacitance [116]. From the studies on six ACs with S_{BET} = 1156–2571 $m^2 g^{-1}$, contribution of surface groups to C_g in 30% KOH as pseudo-capacitance was pointed out to be important [117]. In the case of oxygen-containing functional groups, pseudo-capacitance is generally credited with faradaic reactions of these groups with electrolyte ions, which is basically identical with the capacitance developed by transition metal oxides, such as RuO_2 and MnO_2. However, as described in the section for nitrogen-containing carbons, the origin of increasing capacitance is not quite as simple as stated.

Oxygen-containing functional groups are simply formed by activation [118,119], and deliberately introduced on the surface of carbon by oxidation in O_2 [120,121] or HNO_3 [122,123] and by electrochemical oxidation [123,124]. Oxygen species on the surface are ill-received for the carbon materials used in non-aqueous electrolyte solutions, because they have adverse effects on the reliability of capacitors in regard to voltage proof, self-discharge, leakage current, and others. Substantial costs are consumed to remove oxygen in production of activated carbons for commercial EDLCs. In contrast, oxygen-containing functional groups increase the total capacitance in aqueous electrolyte solutions, in a vast majority of instances in H_2SO_4 solutions, by developing pseudo-capacitance.

The surface oxygen species are classified into two groups by temperature programmed desorption (TPD), the functional groups desorbed as CO (CO-desorbing complexes) and those desorbed as CO_2 (CO_2-desorbing complexes) [118–120,125]. These two groups were found to show different functional capability by a study on PAN-based carbon fibers oxidized in a hot nitric acid solution followed by heat treatment at HTT between 150 and 750 °C in N_2 [122,125]. The value of C_g reached a maximum after 450 °C treatment, which was parallel to the results by TPD that the evolution of CO showed a maximum at 450 °C but the evolution of CO_2 became very few above 450 °C. The values of C_g measured at two different discharge rates were closely related to [CO–CO_2] evolution: CO-desorbing complexes were supposed to assist the formation of EDLs, but CO_2-desorbing complexes to give a negative effect. The CO-desorbing complexes were deduced to be carboxyl or quinone-type. Their contributions to the total capacitance and to the improvement of cyclability were found also for PAN-based ACFs followed by oxidation at 250 °C in O_2 [120]. Electrochemical pretreatment of PAN-based ACF in a $NaNO_3$ solution was reported to increase the content of oxygen-containing functional groups on the fiber surface and consequently to increase C_g [124]. The ACF oxidized for 6 h contained 1.31 mmol g^{-1} of O, and 76% of them were evolved as CO. Various carbon materials, including anthracite and different carbon fibers, were activated by KOH, NaOH, CO_2 or steam at 650–750 °C [118]. The values of C_g measured for all carbon materials activated under different conditions were closely related to the concentration of CO-desorbing complexes, that is, CO evolution/S_{BET}. Since carbon materials were activated at the temperature above 450 °C, no evolution of CO_2 occurred during TPD with these carbons. The mesophase pitch prepared by KOH activation and following heat treatment in N_2 showed that C_g decreased with raising post-treatment temperature as a result of reducing oxygen-containing functional groups [119]. It was reported that the pseudo-capacitance due to CO-desorbing complexes was more clearly observed in a H_2SO_4 solution than KOH solution.

In Fig. 12a, CV curves are shown for ACFs in which either –COOH groups (total amount of oxygen-containing groups 1.76 mmol g^{-1}) or phenolic –OH groups (total amount 0.79 mmol g^{-1}) are rich [123]. Content of oxygen-containing functional groups was determined by titration. The ACF rich in –COOH groups shows humps clearly in its CV curve, suggesting the occurrence of faradaic reactions, but the same ACF rich in phenolic hydroxyl group does not show apparent hump in CV.

For ACF prepared from phenol resin and AC from a petroleum coke, the capacitance C_0 in 1 mol dm^{-3} H_2SO_4 at the current density of 0 mA cm^{-2} was estimated by the extrapolation, which was assumed to be the maximum value eliminated the effect of pore structures. Linear relations between C_0 and the total amount of oxygen-containing groups were obtained on both carbon materials, as shown in Fig. 12b [123].

Oxygen-plasma treatment was shown to increase S_{BET} markedly, leading to the increase in C_g [121].

2.4.2. Nitrogen-containing carbon

Recently, nitrogen-containing carbon materials (N-doped carbons) attracted attention because large pseudo-capacitance was obtained even though they did not have a high surface area. If the ratio of C_g to S_{BET}, C_g/S_{BET} (F m^{-2}), is calculated as a measure, it is 0.1–0.15 F m^{-2} for most of the porous carbons and hard to attain 0.2 F m^{-2}. With carbon materials containing nitrogen at certain levels, C_g/S_{BET} readily exceeds this range and becomes more than 10 times of it in the extreme case [126]. Since a high capacitance is not expected in non-aqueous electrolyte solutions, as shown in Table 2, and only when the carbon materials were used as negative electrodes [127], it is likely that protons are associated with the pseudo-capacitance due to nitrogen. However, it was also reported that the capacitance increased in KOH solutions [127,128]. There is a theoretical investigation of the interaction between hydrogen atoms and N-doped carbons using DFT method [129]. Increasing capacitance by nitrogen doping is often attributed to faradaic reactions of the nitrogen-containing functional groups (*e.g.*, [130]), similar to the case of oxygen-containing carbons. For most of the N-doped carbons, however, the nitrogen content is not sufficiently high to explain large gain in capacitance. Additional rationales are offered such as improving wettability of the pore walls by the formation of polar functional groups, increasing capacitance of the space-charge layer due to the increase in carrier concentration, and others (*e.g.*, [131]). At present, it is difficult to distinguish and determine each contribution, and to explain the effect of nitrogen doping reasonably.

Carbonization, ammoxidation and steam activation were applied in different orders to brown coals and regenerated cellulose fibers [132–134]. However, the nitrogen content of resulting carbon materials was less than a few mass percents and C_g/S_{BET} was much less than 0.2 F m^{-2}. It seems that the increase in S_{BET} rather than incorporating nitrogen contributed to the capacitance. Recent approach using urea treatment and KOH activation showed similar results: practically no effect of nitrogen observed in a H_2SO_4 solution, and the material without urea treatment showed the maximum capacitance [127].

The N-doped carbons that show considerably large capacitance are divided into two groups depending on S_{BET}, ones having very small S_{BET} (<100 $m^2 g^{-1}$) and the others having relatively large S_{BET} (>400 $m^2 g^{-1}$). The first group includes carbons made from pyridine and quinoline using mica templates [135], carbonized melamine foam [126], and carbonized polyaniline [136]. Since the contribution from electric double-layers is minimal, pseudo-capacitance makes up a substantial portion of the total capacitance, leading to very large C_g/S_{BET}. The second group includes those prepared by a variety of procedures, such as carbonization of polymers containing nitrogen [127], various template methods with organic compounds containing nitrogen [128,130,139,64,140], treatment

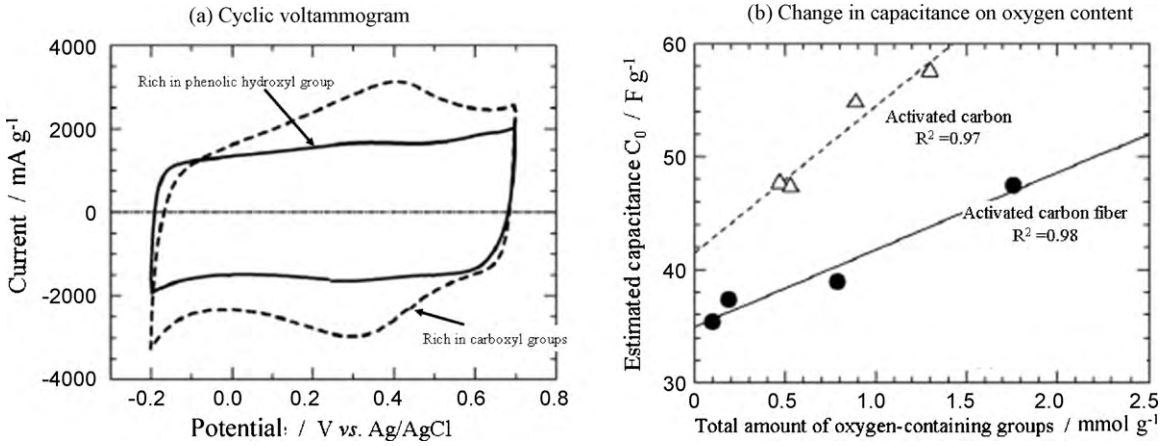

Fig. 12. Cyclic voltammograms for activated carbon fibers rich in either carboxyl or phenolic hydroxyl groups (a) and the relation between extrapolated capacitance C_0 and total amount of oxygen in activated carbon and activated carbon fibers (b) (courtesy of Prof. H. Oda of Kansai Univ.) [123].

with urea or melamine [127,125] and others [132–134]. Large pseudo-capacitance due to nitrogen is commonly recognized by the characteristic shape of CV curve in aqueous electrolyte solutions, that is, non-rectangular shape, which shows enhanced capacitance in the negative potential side due to adsorption of cations, and unnoticeable or very small current humps, as shown in Fig. 13. Most carbon materials belonging to the second group have relatively large S_{BET} and some of them do not show the characteristic shape of CV curve (*e.g.*, [137,141]) or have current humps due to faradaic reactions [139,140] in H_2SO_4 solutions.

Most of these carbon materials have the nitrogen content of 4–10 mass%, though some of them contain more than 20 mass%. As the nitrogen content decreased with raising the temperature for carbonization of precursors, the carbons prepared at 750–900 °C usually showed the best performance. Any activation processes to increase S_{BET} markedly reduced the nitrogen content [43,127,132,137]. Linear relationships between C_g and nitrogen content have been reported in a few individual cases [137,142], but by comparing the data from different references in Table 2 such correlation is difficult to be recognized. One of the reasons is that the contribution of double-layer capacitance is all different. Sometimes, relationship between C_g and nitrogen content was absent but C_g/S_{BET} seemed to be proportional to the nitrogen content (*e.g.*, [140]).

Chemical state of nitrogen in the carbons has been examined by XPS, and mainly four types are detected, namely, pyridinic N, pyrrolic N, quaternary N, and N-oxide [130,133,137,140,141]. Often surface compositions by XPS are reported in the references about carbon materials, but the majority of them are not very reliable, because quantitative capability of XPS is poor for the samples of a rough surface and uneven shape. So far, it is uncertain whether specific nitrogen-functional groups are responsible for pseudo-capacitance. It has been postulated based on the analytical data by wet titration of carbon materials that there is direct relationship between the number of basic groups on the surface and C_g [141]. However, acceptable linearity was observed only at a high current density (1 A g^{-1}) and the results turned out to have a weak side that C_g was not always proportional to the number of basic groups, that is, at a low current density (*e.g.*, 50 mA g^{-1}) the available number of basic groups especially in pores should increase, but C_g did not follow that.

2.4.3. Boron-containing carbons

Development of pseudo-capacitance by boron-doping into carbon materials is not well established. This is mainly due to the difficulty in introducing boron atoms into carbon at the carbonization temperatures below 1500 °C. Concerning this topic, only a limited number of references are found [50,143,144]. By thermal diffusion at 2200–2300 °C, a small amount of boron (<1 at%) was doped into MWCNT, but the resultant materials showed lower capacitances than that of the original MWCNT in non-aqueous electrolyte solutions (0.5 mol dm^{-3} $LiBF_4$ or $TEABF_4$/PC) [50]. Boron-doped carbons were prepared using a mesoporous silica template (SBA-15) from sucrose and boric acid, but the boron content was only 0.065 and 0.16 mass% [143]. With boron-doping, C_g did not change, indicating that meaningful contribution of boron to the capacitance was unlikely. Carbon materials with the boron content of 1–3.4 mass% were derived from the glucose-borate complexes synthesized under hydrothermal condition [144]. Boron was found to be present mainly as a form of C–B–O bonding and no sub-

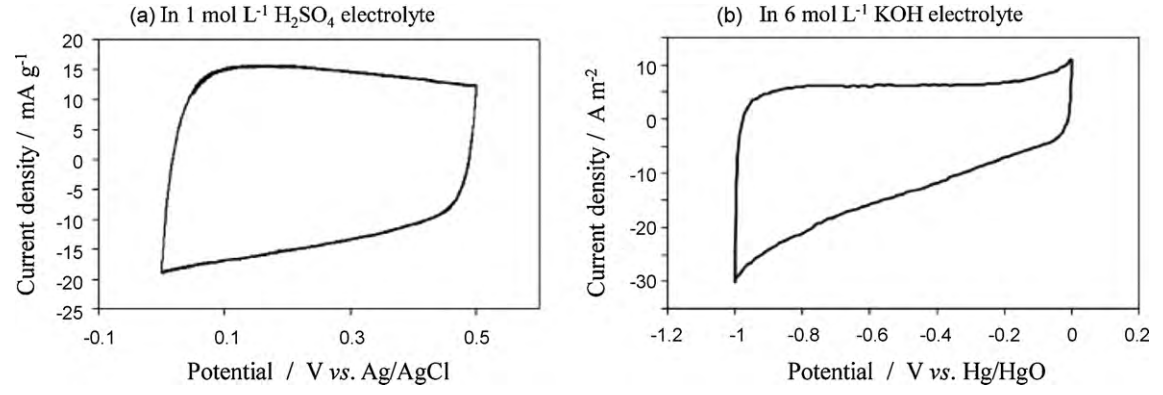

Fig. 13. Cyclic voltammograms for a nitrogen-containing carbon in aqueous electrolytes (courtesy of Dr. M. Kodama of AIST).

Table 3
Carbon used for the construction of asymmetric EDLCs.

Sample code		Precursor	Preparation	Pore structure parameters			
				S_{BET} ($m^2\,g^{-1}$)	S_{micro} ($m^2\,g^{-1}$)	S_{meso} ($m^2\,g^{-1}$)	V_{meso} ($mL\,g^{-1}$)
AC-5	Commercially available	Resin	Activated by steam	1906	1938	113	0.11
AC-2		Resin	Activated by KOH	2216	2144	107	0.09
AC-3		Pitch	Activated by steam	1375	1298	103	0.10
AC-4		Cokes	Activated by steam	1275	1037	561	0.43
CP0	Laboratory-made	Mg citrate	Carbonized at 900 °C for 1 h	1653	160	1780	2.46
CP1		Mg citrate/PVA of 9/1		1382	129	1610	2.40
CP3		Mg citrate/PVA of 7/3		1132	95	1341	1.86
GP0		Mg gluconate		899	685	257	0.23

stituted boron. The CV curves of these materials in a H_2SO_4 solution showed plural humps at different potential regions but no humps in a neutral solution, indicating the occurrence of faradaic reactions related to protons. It is likely that =B–OH type functional groups, which have different functionality from phenolic –OH groups, are involved in the reactions. However, obvious relationship between C_g and the boron content was not observed, because of relatively large S_{BET} of 850–1360 $m^2\,g^{-1}$, which made it difficult to separate the effect of boron-doping.

Recently, boron and nitrogen co-doped carbon materials were reported for electrochemical capacitors [145,146]. The co-doped porous carbons were derived from gels which were prepared from citric acid, H_3BO_3 and NH_4OH using $NiCl_2$ as an activating agent [145]. Composition was estimated by XPS and only three sets were presented. Of the three, a maximum ratio of C_g/S_{BET} of 0.45 $F\,m^{-2}$ was obtained with the material having ~9.6 at% B, ~9.2 at% N, ~17.3 at% O, and S_{BET} of 505 $m^2\,g^{-1}$, but the largest C_g, 247 $F\,g^{-1}$ by CV, was attained with that having ~8.4 at% B, ~7.1 at% N, ~14.7 at% O, and S_{BET} of 894 $m^2\,g^{-1}$. The CV curves in a KOH solution showed very broad bulge both in anodic and cathodic regions. Any correlation between capacitance and composition was absent, and the effect of boron and nitrogen was not discussed in detail. More simple method to form the co-doped carbons was reported, that is, carbonization of the precursor prepared by drying a solution mixture of polyacrylamide (PAA) and H_3BO_3, followed by boiling in water to remove borate by-products [146]. The boron content increased linearly from 4.8 to 18.6 mass% in a range of carbonization temperature of 800–1200 °C, in parallel with the change in the relative intensity of B 1 s peak to C 1 s peak by XPS. Large and broad faradaic peaks arisen from plural reactions appeared in CV curves in a H_2SO_4 solution for the products obtained above 1000 °C. These faradaic peaks disappeared in the neutral electrolytes. By comparing the CV curve with that for nitrogen-containing carbon formed from PAA by the MgO-template method [140], the capacitance due to the faradaic reactions of >B–N< and C–B–O components in the co-doped carbons with protons was found to be added to commonly observed pseudo-capacitance for nitrogen-doped carbons. The values of C_g were 300–305 $F\,g^{-1}$ for the carbons prepared in a temperature range of 850–950 °C. As S_{BET} was 410–420 $m^2\,g^{-1}$ in this range, C_g/S_{BET} reached relatively high values as 0.72–0.74 $F\,m^{-2}$. Since C_g/S_{BET} was 0.32 $F\,m^{-2}$ in Na_2SO_4 and Li_2SO_4 solutions for the carbon prepared at 900 °C, cations Na^+ and Li^+ were supposed to contribute also to the development of pseudo-capacitance, though it is not as a faradaic reaction. With raising carbonization temperature, C_g and the ratio C_g/S_{BET} started to decrease from around 1000 °C. It was attributable to the formation of h-BN by-products from the results by XPS, FT-IR and XRD. A modification of resorcinol-formaldehyde-derived cryogel by ammonia borane was reported to give boron and nitrogen co-doped carbon, but the nitrogen content was very small as 0.1 at%, even though boron content was 2.5 at% with relatively high oxygen content of 8.8 at% [147].

2.4.4. Metal dispersed carbons

Ruthenium oxide RuO_2 was found to give a high capacitance in aqueous electrolyte solutions [148–150]. Different trials to reduce the amount of expensive RuO_2 by keeping its high capacitance have been carried out, chemical vapor deposition of Ru [151], hydrolysis of $RuCl_3$ [152], electroless deposition of Ru metal in a $RuCl_3$ aqueous solution [153], etc. Ru loading onto a carbon black, which was done through colloidal aqueous solution of $RuCl_3$ by adding appropriate amount of $NaHCO_3$, was reported to give a maximum capacitance from 221 to 599 $F\,g^{-1}$ with the increase in amount of Ru from 20 to 80 mass% [154].

Replacement of expensive RuO_2 by other inexpensive metals, such as MoO_3 and Fe_3O_4, was also reported to give certain benefit [155–157]. Dispersion of transition metals in carbon through carbonization of polyimide films containing 0.1–2 at% metals was carried out and marked increase in capacitance in H_2SO_4 was observed [158].

Carbon-coated WC and Mo_2C, which were prepared from the mixtures of a carbon precursor with K_2WO_4 and K_2MoO_4 by the heat treatment at a temperature between 800 and 1050 °C in Ar gas, were found to give a high capacitance in H_2SO_4 [159]. WC and Mo_2C were converted to oxy-hydroxides during the 1st cycle of charge–discharge.

3. New configuration using carbons

Various capacitors were tested by using different materials in their positive and negative electrodes and called asymmetric capacitors. In the asymmetric capacitors reviewed here, a carbon material was used at least in one of electrodes, where the formation of EDL is the principal mechanism for electric energy storage. The capacitors, of which another electrode is composed of another carbon material and the main mechanism is also EDL formation, are called asymmetric EDLCs. When the main mechanism in another electrode of either metal or polymer is redox reaction, the capacitors are called hybrid ones.

3.1. Asymmetric EDLCs

Asymmetric EDLCs were constructed by using a combination of a microporous carbon with different mesoporous carbons [160,161]. In Table 3, carbons used are listed with their pore parameters, together with their origins. Asymmetric EDLCs consisting of the negative electrode of the microporous activated carbon AC-5 with the positive electrode of different carbons XX, AC-5 itself and from CP0 to GP0, were expressed as AC-5/XX, and those of positive electrode of AC-5 with negative electrode of carbon XX was expressed as XX/AC-5.

In Fig. 14a and b, the capacitance C_g measured in a two-electrode test cell of 1 mol L^{-1} $TEMABF_4$/PC with current densities of 100 and 1000 mA g^{-1}, respectively, are plotted against the ratio in S_{BET} of negative to positive electrode carbons, S_{BET} (negative)/S_{BET} (posi-

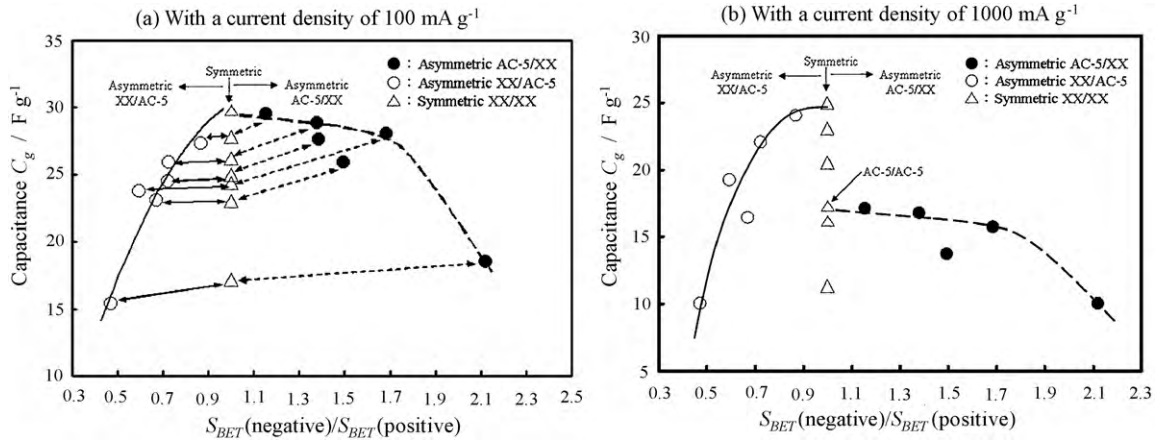

Fig. 14. Relations between capacitance C_g in 1 mol L^{-1} $TEMABF_4$/PC and the ratio of S_{BET} of negative electrode carbon to S_{BET} of positive electrode carbon on asymmetric and symmetric capacitors with two current densities [160].

tive) (hereafter, S_{BET} ratio), for the asymmetric capacitors AC-5/XX and XX/AC-5. In these figures, the capacitance measured on symmetric capacitors XX/XX are also plotted at the position of S_{BET} ratio of 1.0, and the experimental points measured on the same carbon XX in the negative and positive electrodes are connected by solid and dotted lines, respectively. In these figures, the left hand side from the position for symmetric capacitors (*i.e.*, S_{BET} ratio = 1.0) shows how the capacitance changes with the change of negative electrode carbon and the right hand side shows the effect of positive electrode change on capacitance.

On the right hand side (*i.e.*, AC-5/XX) with the current density of 100 mA g^{-1} (Fig. 14a), capacitance decreases gradually when the S_{BET} ratio increases from 1.0, *i.e.*, S_{BET} of the positive electrode carbon decreases. Above the S_{BET} ratio of more than 1.7, however, it seems to decrease rapidly. By increasing charge/discharge rate to 1000 mA g^{-1} on asymmetric capacitors AC-5/XX, the relation between capacitance and S_{BET} ratio changes markedly, as shown in Fig. 14b. Capacitance becomes almost constant even though carbon in the positive electrode was changed, which is very similar value of that of the symmetric capacitor constructed from the microporous AC-5.

On the left hand side (*i.e.*, XX/AC-5), capacitance decreases rapidly with decreasing S_{BET} ratio with both current densities of 100 and 1000 mA g^{-1}. The capacitance values measured on XX/AC-5 are very similar to those on symmetric XX/XX. These results on XX/AC-5 are due to the following fact that the positive electrode has enough surface area to accommodate the number of anions balanced with that of cations adsorbed in the negative electrode, because the positive electrode carbon AC-5 has high surface area enough to accommodate anions, which can be balanced with the cations adsorbed into the negative electrode. It has to be mentioned that the increase in current density from 100 to 1000 mA g^{-1} does not change the tendency on C_g *vs.* S_{BET} ratio on the asymmetric XX/AC-5, although a marked change is observed on AC-5/XX.

In Fig. 15a, performance rating expressed by the ratio of capacitance with 1000 mA g^{-1} to that with 100 mA g^{-1}, C_{1000}/C_{100}, is plotted against S_{BET} ratio. On AC-5/XX, performance rating C_{1000}/C_{100} is very low and almost constant of about 55%. On XX/AC-5, however, C_{1000}/C_{100} depends strongly on S_{BET} ratio, *i.e.*, on negative electrode carbon. The results on asymmetric capacitors shown in Fig. 14 suggest that both capacitance and rate performance are predominantly governed by the pore structure of carbon material in the negative electrode.

In Fig. 15b, therefore, performance rating C_{1000}/C_{100} is plotted against S_{meso} of negative electrode carbon, in which the results on another series of asymmetric capacitors using a microporous carbon AC-2 are included. A good linear relation between C_{1000}/C_{100} and S_{meso} (negative electrode) suggests that rate performance of EDLCs is governed also by the negative electrode carbon, particularly by its mesoporous surface area; in order to have a high performance rating a high S_{meso} in negative electrode carbon is desired. By using mesoporous carbon with relatively high S_{meso} as

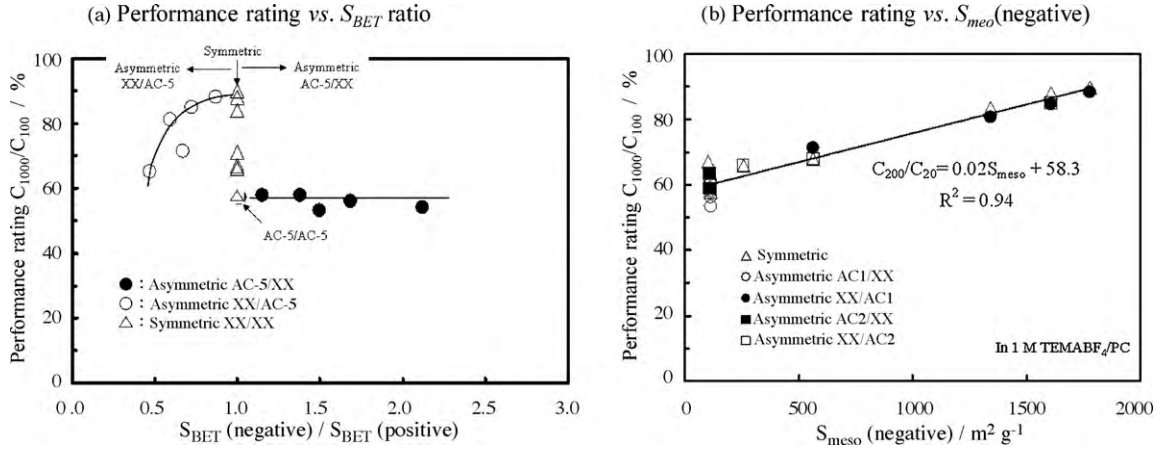

Fig. 15. Performance rating C_{1000}/C_{100} against the ratio of S_{BET} (negative)/S_{BET} (positive) (a) and mesoporous surface area S_{meso} of negative electrode carbon (b) in asymmetric and symmetric capacitors [160].

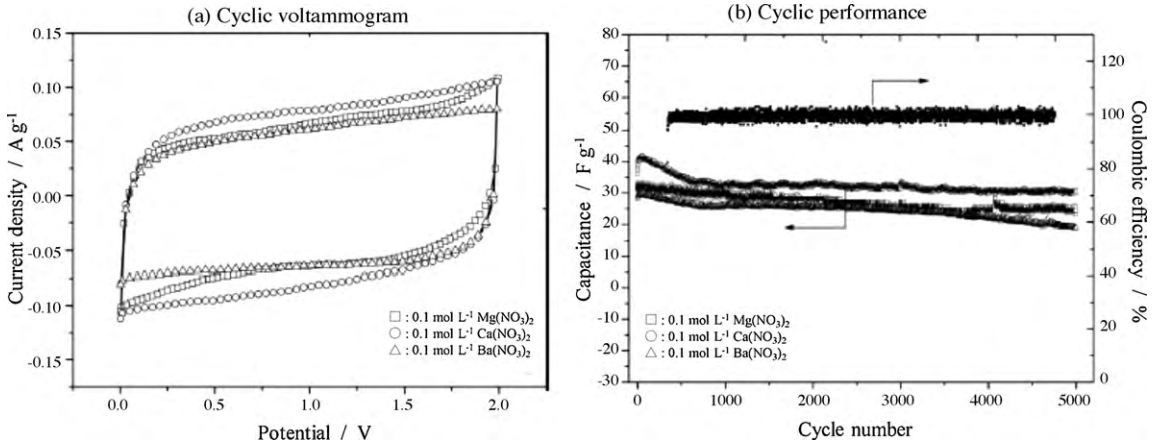

Fig. 16. Cyclic voltammograms and cyclic performances of a hybrid capacitor composed from activated carbon in the negative electrode and amorphous hydrous MnO_2 in the positive electrode in the aqueous solution of different metal nitrates (courtesy of Prof. F. Kang of Tsinghua Univ.) [170].

1700 $m^2\,g^{-1}$, high performance rating close to 90%, *i.e.*, 90% retention by increasing current density from 100 to 1000 $mA\,g^{-1}$, can be attained.

An asymmetric EDLC constructed from the negative electrode composed of a mesoporous pitch-derived activated carbon and the positive electrode of its 1000 °C-treated one was reported to have a good cyclability in 1 $mol\,L^{-1}$ H_2SO_4 with a current density of 500 $mA\,g^{-1}$: capacitance of 220 $F\,g^{-1}$ for the first cycle, 210 $F\,g^{-1}$ after 10,000 cycles and 200 $F\,g^{-1}$ after 20,000 cycles [162].

Asymmetric construction of EDLC gives a merit to employ different carbon materials in different electrode. For obtaining a high capacitance at a low current density in $TEMABF_4$/PC, a highly microporous carbon is needed at the negative electrode, but at the positive electrode less porous carbon can be used, which might be less expensive. For a high rate performance, a mesoporous carbon is desired at the negative electrode.

3.2. Hybrid capacitors

Hybrid capacitors consisting of different storage mechanisms were proposed, electric double-layer formation at the positive electrode and faradaic charge-transfer reaction with Li^+ in the electrolyte at the negative electrode [163–165]. A cell composed of an activated carbon with S_{BET} of 2200 $m^2\,g^{-1}$ at the positive electrode and the carbon with a low S_{BET} of 250 $m^2\,g^{-1}$ at the negative electrode, which was prepared by the heat treatment of the activated carbon with pitch at 700 °C, was reported to have high cyclic performance in 1 $mol\,L^{-1}$ $LiPF_6$/EC/DEC [163]. On a hybrid capacitor composed of a combination of commercial activated carbon (S_{BET} of 1500 $m^2\,g^{-1}$) and nongraphitizable carbon (S_{BET} of 4.5 $m^2\,g^{-1}$) as the positive and negative electrodes, respectively, high energy and power densities (81.4 $W\,h\,L^{-1}$ and 8567 $W\,L^{-1}$, respectively) were obtained by extending potential range from 1.5 to 4.3 V in 1 $mol\,L^{-1}$ $LiPF_6$/EC/DEC [164]. In order to extend the potential range, a preliminary charging process using auxiliary Li electrode in the cell, *i.e.*, doping of Li into nongraphitizable carbon of the negative electrode, was necessary, of which energy seemed to correspond to the irreversible capacity for nongraphitizable carbon in lithium ion rechargeable batteries. Energy and power densities became 1.14 and 2.3 times higher by extending the potential range from 2.5–4.3 to 1.5–4.3 V. Similar hybrid capacitors were tested in various nonaqueous solutions of lithium salt electrolytes [165].

Hybrid capacitors constructed by using an activated carbon in the negative electrode and MnO_2 in the positive electrode were proposed, which had to be operated below 1.5 V in order to avoid the evolution of hydrogen and oxygen on the negative and positive electrode, respectively [166–168]. A composite of amorphous $MnO_2{\cdot}nH_2O$ with carbon nanotubes (15 mass%) as the positive electrode coupled with activated carbon negative electrode was reported to extend the operating cell voltage up to 2 V, in which hydrogen formed by water decomposition at the negative electrode was supposed to be adsorbed into micropores of activated carbon and electrochemically oxidized during discharge cycle [169]. A hybrid capacitor constructed from a positive electrode of an amorphous hydrous MnO_2, which was synthesized from $KMnO_4$ using a surfactant as dispersant and reductant [170], with a negative electrode of activated carbon gave a high capacitance of 37, 32 and 29 $F\,g^{-1}$ in 0.1 $mol\,L^{-1}$ aqueous solutions of nitrates of alkaline earth metals, Mg^{2+}, Ca^{2+} and Ba^{2+}, respectively [171,172]. These capacitors showed rectangular voltammograms in a potential window from 0 to 2 V, as shown in Fig. 16a and high cyclability over 5000 cycles with a current density of 300 $mA\,g^{-1}$, as shown in Fig. 16b.

A hybrid capacitor was constructed by using mesoporous NiO as positive electrode and $Ni(OH)_2$-templated mesoporous carbon as negative electrode with 6 $mol\,L^{-1}$ KOH electrolyte [173]. Cyclic voltammograms of this asymmetric capacitor showed that the main storage mechanism seems to be the formation of EDL up to 0.8 V with a small hump due to redox reactions and becomes more marked redox reactions on the surface of NiO electrode with increasing potential to 1.5 V. In an potential window of 1.0–1.5 V, capacitive performance is governed by NiO electrode and the capacitance value depends strongly on sweep rate, even though the capacitance is relatively high.

Capacitive performance of a hybrid capacitor of an activated carbon with a poly(4-fluorophenyl-3-thiophene) was studied in 1 $mol\,L^{-1}$ $TEACF_3SO_3$/AN [174]. The performance of large prototype capacitor with the electrode area of 60 cm^2 was constructed with 1 $mol\,L^{-1}$ $TEABF_4$/PC electrolyte. A combination of carbon negative electrode with poly(3-methylthiophene) positive electrode was also studied in ionic liquid electrolytes [175,176]. A hybrid capacitor with polyfluorene/carbon black (Ketjen black) composite as positive electrode and activated carbon (S_{BET} of 1600 $m^2\,g^{-1}$) as negative electrode gave a higher capacitance and better cyclability than the symmetric capacitor with the same activated carbon [177].

A hybrid capacitor was proposed by using activated carbon as the positive electrode and $Li_4Ti_5O_{12}$ as the negative electrode with $LiPF_6$/EC/DMC [178]. It shows a sloping voltage profile in a range of 1.5 and 3 V, which is due to faradaic reaction between negative electrode material and Li^+ in the electrolyte, and good cyclic performance with about 10% loss after 5000 cycles. Prototypes of this asymmetric capacitor with a capacitance of 500 F and a weight of

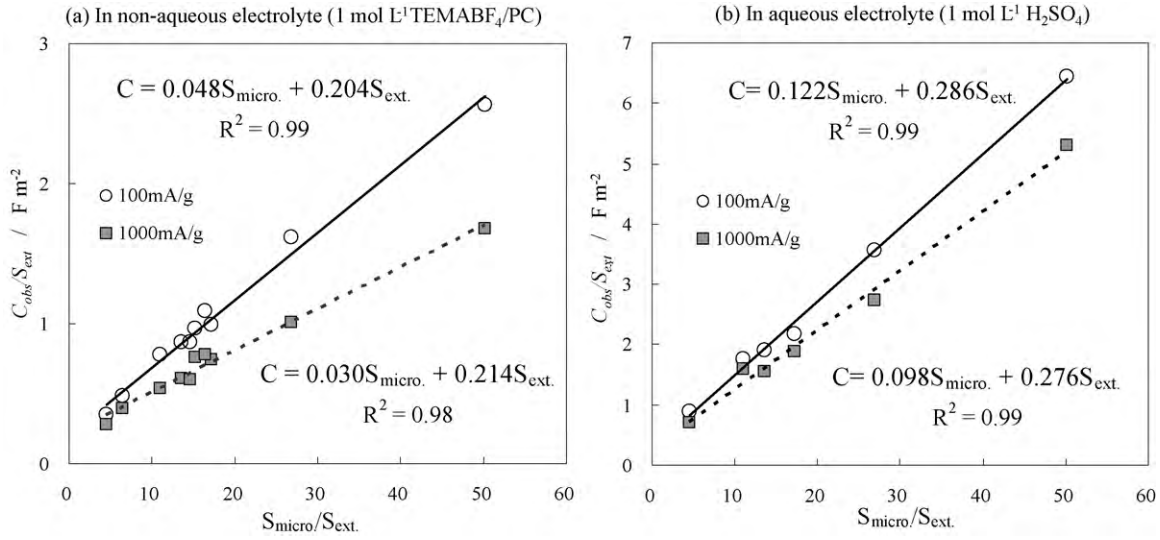

Fig. 17. Relations between C_{obs}/S_{ext} and S_{micro}/S_{ext} for various activated carbons in non-aqueous and aqueous electrolyte solutions with two current densities [181].

43 g were built, which had an energy density of 10.4 W h kg^{-1}, a power density of 793 W kg^{-1} at 95% discharge efficiency, and long cycle life up to 10^5 cycles [179,180].

Hybrid capacitors were studied by aiming the improvement in performance. However, they are not yet forwarded to the practical application mainly because the performance improvement is not marked enough and/or because the cost of the electrode materials increases.

4. Discussions

4.1. Formation of electric double-layer on carbon surface

In electrochemical capacitors which are discussed above, the formation of electric double-layers on the surface of electrode carbon is the principal mechanism. Therefore, high surface area is preferable for getting high capacitance of EDLCs, but a definite relation between the observed capacitance and S_{BET} has never been obtained. It was pointed out that the determination of the real surface area is very important to understand the EDLC performance of electrode carbons and it should not be limited to S_{BET}, being recommended to use various techniques; analyses of N_2 adsorption/desorption isotherms by different techniques and immersion enthalpy measurements [74].

Capacitance observed C_{obs} (F g^{-1}) was analyzed by dividing into two parts, capacitance due to the surface of micropores S_{micro} and that due to the surface of larger pores (mesopores and macropores) which was measured as the external surface area S_{ext}, as follows [20]:

$$C_{obs} = C_{ext} \times S_{ext} + C_{micro} \times S_{micro}, \quad (1)$$

where C_{micro} and C_{ext} are the capacitance per 1 m^2 area of micropore and that of other larger pores, respectively (*i.e.*, capacitance contributions of micropore surface and other larger pore surface, respectively, and expressed in the unit of F m^{-2}). Here it has to be pointed out that S_{ext} is governed predominantly by mesopores and so can be replaced by S_{meso}. Eq. (1) was rewritten to

$$\frac{C_{obs}}{S_{ext}} = C_{ext} + C_{micro}\left(\frac{S_{micro}}{S_{ext}}\right), \quad (2)$$

which suggests the linear relation between (C_{obs}/S_{ext}) and (S_{micro}/S_{ext}), both parameters being experimentally determined. In Fig. 17, the corresponding plots are shown for various activated carbons, covering a wide range of S_{BET}, S_{micro} and S_{ext} [181,182]. On the same carbons, capacitance was measured in aqueous and non-aqueous electrolyte (1 mol L^{-1} H_2SO_4 and 1 mol L^{-1} TEMABF$_4$/PC, respectively) with different current densities between 100 and 1000 mA g^{-1}. Practically, capacitance measurement in TEMABF$_4$/PC was performed in a two-electrode test cell, but their values were converted to those in three-electrode test cell in order to make comparison with those in H_2SO_4.

The relations between C/S_{ext} and S_{micro}/S_{ext} are well approximated by applying least square calculation to be linear both in the non-aqueous and aqueous electrolytes with different current densities, as shown on two current densities in Fig. 17. The results show that the contributions from micropores and other larger pores to observed capacitance, *i.e.*, C_{micro} and C_{ext}, are different in both non-aqueous and aqueous electrolytes.

In Fig. 18, the dependences of C_{micro} and C_{ext} on current density are shown for the two electrolytes [182]. In the non-aqueous electrolyte, C_{ext} does not show pronounced change with current density and appears to be constant of about 0.21 F m^{-2}, but C_{micro} is very small as 0.04 F m^{-2} and seems to decrease with increasing current density. In the aqueous electrolyte, on the other hand, C_{ext} is also almost constant at about 0.3 F m^{-2}, with a rapid increase at low current density of less than 100 mA g^{-1}, but C_{micro} shows a gradual decrease from 0.15 to 0.1 F m^{-2} by the increase in current density from 20 to 1000 mA g^{-1}. C_{micro} in the non-aqueous electrolyte is much smaller than that in the aqueous electrolyte (about 0.04 and 0.1 F m^{-2}, respectively), though C_{ext} is not so much different in both electrolytes (about 0.2 and 0.3 F m^{-2}). These results were understood by the fact that the sizes of cation of the aqueous electrolyte H^+ are much smaller than that of the present non-aqueous electrolyte TEMA$^+$.

In Table 4, the data on C_{micro} and C_{ext} published in various literatures are summarized, together with carbon material, electrolyte, cell, current density, and the method for the surface area determination used.

The same analysis was applied on various carbon materials [20,23,32,38,181–184,185] and most of the papers are reporting to succeed to evaluate C_{micro} and either C_{ext} or C_{meso}. The conditions for the measurement of capacitance are very much different, different electrolytes with different concentrations and different techniques with different rates. In addition, the method for the evaluation of pore structure is also different, most of the works using N_2 adsorption isotherm but different analy-

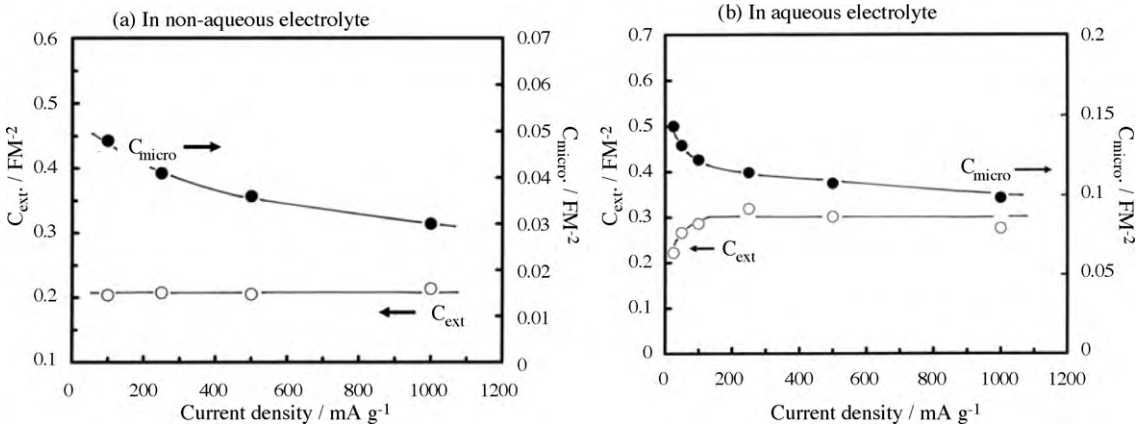

Fig. 18. Dependences of capacitance contribution of microporous surface C_{micro} and that of external surface C_{ext} on current density in non-aqueous and aqueous electrolyte solutions [182].

sis procedures. The analysis using α_s plot of N_2 adsorption was successfully applied to microporous and mesoporous carbons [23,38,181,182,185]. Even though the direct comparison among the data on C_{micro} and C_{ext} is difficult because of so widely different experimental conditions, the ratio C_{ext}/C_{micro} is about 2 in the aqueous electrolyte, but about 4–7 in the non-aqueous electrolyte and charge/discharge rate gives marked effect on C_{micro} than on C_{ext}. C_{micro} and C_{meso} (or C_{ext}) may be called microporous and mesoporous specific capacitances, respectively, in stead of the ratio C/S_{BET} which has been often used. However, our knowledge on C_{micro} and C_{ext} is very limited, as shown in Table 4.

It might be useful to understand the EDLC capacitance by separating the contributions due to the surfaces of pores with different sizes. In the papers referred in Table 4, the pores are differentiated into micropores (<2 nm) and larger pores (>2 nm). However, it might be better to differentiate pores at another size, which is reasonably supposed to depend strongly on the sizes of cation and anion of the electrolyte employed and possibly on the solvent used. Therefore, more detailed studies on various electrolyte solutions are strongly desired.

It was pointed out that carbon in negative electrode may facilitates the adsorption of desolvated or partially desolvated $TEMA^+$ into small micropores and some of adsorbed cations in micropores may stay even after discharging (trapping) [186]. Adsorption of desolvated cations by contacting with both sides of wall of small micropores seems to be possible, being the more probable in the smaller micropores, as illustrated in Fig. 19. In such a case, the capacitance contribution C_{micro} of a cation is reasonably supposed to become a half, because one cation occupies two facing wall surface, which might be the reason why C_{micro} of large-sized cation in non-aqueous electrolyte $TEMA^+$ is much smaller than that of aqueous electrolyte cation H^+ (refer Fig. 18). Also desolvation before cation adsorption into micropores may disturbs quick charging of EDLCs.

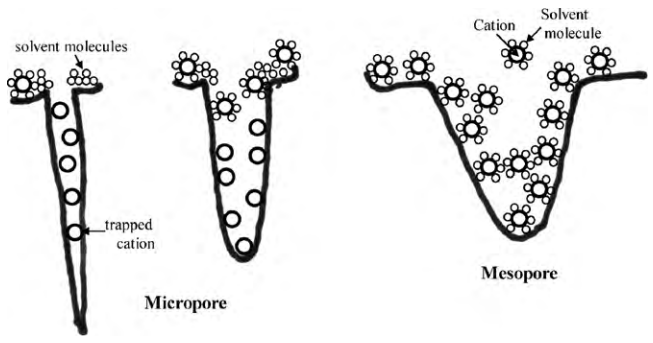

Fig. 19. Schema for adsorption of electrolyte ions with or without solvation to the surface of pores with different sizes.

Cations trapped in micropores was supposed to be so strong that high positive potential was needed to detrapping of these cations, on the basis of the comparison among the capacitances of the fresh electrode carbons, that after trapping of the cations and that after electrochemical detrapping of cations [186]. Trapping phenomenon was tried to explain on the basis of the structure of disordered activated carbons, assuming the presence of three types of micropores: (i) the wall of micropores composed preferentially of basal plane of hexagonal carbon layers, (ii) that mainly of edge planes and (iii) those of both basal and edge planes. Cations are reasonably supposed to be adsorbed somewhat more strongly on the edge planes than on the basal planes, and so the micropores of type (ii) trap $TEMA^+$ so strongly that detrapping is difficult by ordinary discharge process and those of type (iii) trap $TEMA^+$ a little stronger than those of type (i).

It has to be pointed out here that Eq. (1) was applied on the carbons with randomly aligned pores. For the carbon materials having ordered micro- and mesopores prepared through template processes, as described in Section 2.2.4, the applicability of Eq. (1) was not confirmed. There might need some modifications to understand the observed capacitance by using the contributions from different pore surfaces. Mesopore aspect ratio, *i.e.*, the ratio of length to diameter of ordered mesopores, was reported to determine the transport of electrolyte ions [187].

4.2. Contributions of pseudo-capacitance

All carbon materials contain certain amount of functional groups, most of them being reasonably supposed to be bonded with carbon atoms on edge surface and neighboring at structural defects, most of them containing oxygen in the form of –OH, =CO, –COOH, etc. Some of these functional groups, not only containing oxygen but also nitrogen, were known to give additional capacitance to electric double-layer capacitance, as explained in Section 2.4.

It was reported that observed capacitance changes linearly with the amount of CO-desorbing functional groups determined by TPD and does not depend on CO_2-desorbing groups [118,122,125]. A quantitative evaluation of pseudo-capacitance due to nitrogen-containing functional groups has not yet been reported. A proposal to get overall assessment on the capacitance measured with a low current density as 1 mA cm^{-2} to depend on the total surface area and on the amount of functional groups generate CO, [CO], was presented on a large number of porous carbons, including ACs [188].

Table 4
Reported data on the contributions of microporous and external surfaces, C_{micro} and C_{ext}, on EDLC capacitance.

Electrode carbon	EDLC measurement			Surface area determination	Capacitance contribution of pore surfaces ($F\,m^{-2}$)		C_{ext}/C_{micro}	Reference
	Electrolyte	Test cell	Current or scan rate		Microporous surface, C_{micro}	External surface, C_{ext}		
Microbeads	30 mass% KOH	Two-electrode cell	5 mA	DFT	0.195	0.74	3.8	[20]
Carbon fibers					0.145	0.075	0.5	
Activated carbons from coals	6 mol L^{-1} KOH	Two-electrode cell	160 mA g^{-1}	C_6H_6 Adsorption	0.101	0.091	0.9	[183]
	1 mol L^{-1} H_2SO_4	Three-electrode cell	2 mV s^{-1}		0.098	0.231	2.4	
Cypress charcoal	1 mol L^{-1} H_2SO_4	Three-electrode cell	50 mA g^{-1}	α_s	0.17	0.28	1.4	[38]
			1000 mA g^{-1}		0.13	0.18	1.2	
Activated carbons	1 mol L^{-1} H_2SO_4	Three-electrode cell	100 mA g^{-1}	α_s	0.12	0.29	2.4	[181]
			1000 mA g^{-1}		0.10	0.28	2.8	
Nanoporous glassy carbon	6 mol L^{-1} KOH	Two-electrode cell	40 mA g^{-1}	BET and *t*-plot	0.18	0.0039	0.16	[184]
			3000 mA g^{-1}		0.062	0.23	3.7	
Activated carbons	1 mol L^{-1} $TEMABF_4$/AN	Three-electrode cell	20 mV s^{-1}	BET and DFT	0.076	−0.086	–	[32]
Activated carbons	1.2 mol L^{-1} $TEMABF_4$/AN	Two-electrode cell	10 mV s^{-1}	α_s	0.121	−0.112	–	[23]
Activated carbons	1 mol L^{-1} $TEMABF_4$/PC	Two-electrode cell	20 mA (100 mA g^{-1})	α_s	0.05	0.20	4.3	[181]
			200 mA (1000 mA g^{-1})		0.03	0.21	7.2	
Air-oxidized carbon spheres	1 mol L^{-1} $TEMABF_4$/PC	Two-electrode cell	20 mA (100 mA g^{-1})	α_s	0.017	0.187	11.0	[185]
			200 mA (1000 mA g^{-1})		0.008	0.116	14.5	

The relation was formulated as follows:

$$C\,(\mathrm{F\,g^{-1}}) = 0.081 S_{\mathrm{total}}\,(\mathrm{m^2\,g^{-1}}) + 63\,[\mathrm{CO}]\,(\mathrm{mmol\,g^{-1}}). \quad (3)$$

However, it has to be pointed out that this equation is valuable in 2 mol L^{-1} H_2SO_4. Since the capacitance value strongly depends on electrolyte and its concentration, more detailed studies by using various carbon materials and electrolyte solutions are required.

In Eq. (1) [20,182], pore structure in electrode carbon is focused, but surface chemistry of carbon, which causes pseudo-capacitance, is neglected. In Eq. (3) [187], on the other hand, pseudo-capacitance due to oxygen-containing functional groups is separated from the capacitance due to the formation of double-layer, which is governed by pore structure of electrode carbon, but the difference in the contributions of different pores, micropores and other large pores, are not taken into consideration. Therefore, a noble equation has to be developed, which includes both parameters depending on the pore structure of electrode carbon, such as C_{micro} and C_{ext}, and those due to functional groups containing oxygen and nitrogen.

4.3. Keys for electrochemical capacitors

In the previous Sections 2.1–2.4, 3.1 and 3.2, the experimental results on capacitive performance of various carbon materials are summarized. Regrettably, specific capacitance value was impossible to be assigned to each carbon materials, because capacitance strongly depends on the following conditions: (1) conditions of the electrochemical measurement, such as electrolyte solution, its concentration, temperature of measurement, rate of charge/discharge, test cell (either two- or three-electrode cell), etc., and (2) electrode sheet preparation, such as amount of sample carbon in the sheet, what is binder, use of conductive additive or not, density and thickness of the sheet, and so on. In many of the papers published, one electrolyte in either two- or three-electrode cell was used for limited number of carbons or limited range of preparation condition.

Theoretically, EDLC capacitance depends also on pore structure of electrode carbons even if the conditions for the measurements mentioned above were kept exactly the same. The characterization of pore structure of carbon materials was also carried out by different methods. In most of the papers, adsorption isotherm of N_2 gas at 77 K was measured and analyzed by BET method to calculate S_{BET}. However, S_{BET} is known to be not an appropriate parameter to explain observed capacitance, as discussed previously. In order to get more detailed information on pore structure in carbon materials, it is required to analyze the adsorption isotherms by using another method, which has not been established for applying to EDLC capacitances, DFT method in some papers, α_s plot in other papers, and so on. It was recommended to carry out the surface area evaluation through immersion enthalpy of various organic molecules, in addition to the analysis of N_2 gas adsorption isotherm [74]. Most of the papers published do not present sufficient information on the pore structure in the carbon materials used, some papers giving only S_{BET}, some papers volumes of micropores and mesopores but not their surface areas, etc.

On the basis of this discussion, the present authors would like to emphasize the necessity of the specification for the measurements of capacitive performance of electrochemical capacitors, which can be internationally accepted from scientists and engineers who are working on capacitors. The followings have to be specified: the electrolyte solution (possibly one from aqueous and another from non-aqueous electrolytes, their concentrations, the solvent for non-aqueous electrolyte, and temperature of measurement), the electrode sheet (particle size of sample carbon, electro-conductive additives, binder, their mixing ratio, thickness, size and density of the sheet, and also current collector), and the electrochemical measurement (how to calculate capacitance whether from a slope or an integrated area, potential range to be measured, current

density, and measurement of cyclic performance), although galvanostatic measurement with a constant current is recommended than cyclic voltammetry. It is recommended to use both two- and three-electrode test cells on the same electrode carbon. In the case of two-electrode test cell it has to be specified how the capacitance is expressed per mass of carbon material, that is, the observed electric quantity has to be divided by the total mass of carbon materials used in two electrodes, in other words, the sum of carbon materials used in both negative and positive electrodes.

Together with the above-mentioned specifications, it might be useful to select a reference carbon material, of which the capacitance value and pore structure are well established, and recommend the researchers to present its capacitance value in each report to demonstrate the reliability of their capacitance measurements.

5. Concluding remarks

Carbon materials used in EDLCs were reviewed by referring a wide range of materials, porous carbons prepared by various processes, including carbon nanotubes, and carbons containing foreign atoms. Unfortunately, we could not assign the specific capacitance to each carbon materials, because so much different conditions were employed for the determination of capacitive performance of EDLCs and also in some cases enough information on pore structure of electrode carbons was not presented. On the basis of the present situation, the necessity of internationally accepted specification for the determination of capacitive performance was emphasized.

The results on asymmetric EDLCs, predominant contribution of the negative electrode carbon and its mesopores on capacitive performance and differentiation to the contributions of microporous and mesoporous surfaces C_{micro} and C_{ext} to capacitance may give important suggestions for designing the EDLCs.

Acknowledgement

The authors would like to express their sincere thanks for the persons who permit to use their data in figures.

References

[1] R. Parsons, Chem. Rev. 90 (1990) 813.
[2] S. Sarangapani, P. Lesener, J. Forchione, A. Griffith, A.B. LaConti, J. Power Sources 29 (1990) 355.
[3] B.E. Conway, Electrochemical Supercapacitors, Kluwer Academic/Plenum Publishers, 1999.
[4] E. Frackowiak, F. Beguin, Carbon 39 (2001) 937.
[5] A.G. Pandolfo, A.H. Hollenkamp, J. Power Sources 157 (2006) 11.
[6] P. Simon, A. Burke, Interface 17 (1) (2008) 38.
[7] F. Beguin, E. Frackowiak (Eds.), Carbon Materials for Electrochemical Energy Storage Systems, CRC Press, 2009.
[8] M. Ue, J. Electrochem. Soc. 141 (1994) 3336.
[9] M. Arulepp, L. Permann, J. Leis, A. Perkson, K. Rumma, A. Jaenes, E. Lust, J. Power Sources 133 (2004) 320.
[10] M. Morita, T. Kaigaishi, N. Yoshimoto, M. Egashira, T. Aida, Electrochem. Solid-State Lett. 9 (2006) A386.
[11] E. Lust, G. Nurk, A. Jaenes, M. Arulepp, P. Nigu, P. Moeller, S. Kallip, V. Sammelselg, J. Solid State Electrochem. 7 (2003) 91.
[12] M. Lazzari, M. Mastragostino, F. Soavi, Electrochem. Commun. 9 (2007) 1567.
[13] M. Mastragostino, F. Soavi, J. Power Sources 174 (2007) 89.
[14] X. Liu, T.J. Osaka, J. Electrochem. Soc. 143 (1996) 3982.
[15] X. Liu, T.J. Osaka, J. Electrochem. Soc. 144 (1997) 3066.
[16] L. Eliad, G. Salitra, A. Soffer, D. Aurbach, J. Phys. Chem. B 105 (2001) 6880.
[17] M. Endo, T. Maeda, T. Takeda, Y.J. Kim, K. Koshiba, H. Hara, M.S. Dresselhaus, J. Electrochem. Soc. 148 (2001) A910.
[18] S. Shiraishi, TANSO No. 228 (2007) 195.
[19] M. Inagaki, New Carbon Mater. 24 (2009) 193.
[20] H. Shi, Electrochim. Acta 41 (1996) 1633.
[21] D. Qu, H. Shi, J. Power Sources 74 (1998) 99.
[22] H. Yang, M. Yoshio, K. Isono, R. Kuramoto, Electrochem. Solid-State Lett. 5 (2002) A141.
[23] A. Jänes, H. Kurig, E. Lust, Carbon 45 (2007) 1226.
[24] A. Braun, M. Baertsch, B. Schnyder, R. Koetz, O. Haas, H.-G. Haubold, G. Goerigk, J. Non-Cryst. Solids 260 (1999) 1.
[25] H. Teng, Y. Chang, C. Hsich, Carbon 39 (2001) 1981.
[26] T.C. Weng, H. Teng, J. Electrochem. Soc. 148 (2001) A368.
[27] M. Endo, Y.J. Kim, T. Maeda, K. Koshiba, K. Katayama, M.S. Dresselhaus, J. Mater. Res. 16 (2001) 3402.
[28] D.L. Lozano-Castello, D. Cazorla-Amoros, A. Linares-Solano, S. Shiraishi, H. Kurihara, A. Oya, Carbon 41 (2003) 1765.
[29] K. Kierzek, E. Frackwiak, G. Lota, G. Gryglewicz, J. Machnikowski, Electrochim. Acta 49 (2004) 515–523, Erratum, Electrochim. Acta 49 (2004) 1169.
[30] R. Asakura, T. Kondo, M. Morita, H. Hatori, Y. Yamada, TANSO No. 215 (2004) 231.
[31] Y.J. Kim, Y. Horie, S. Ozaki, Y. Matsuzawa, H. Suezaki, C. Kim, N. Miyashita, M. Endo, Carbon 42 (2004) 1491.
[32] O. Barbieri, M. Hahn, A. Herzog, R. Koetz, Carbon 43 (2005) 1303.
[33] M. Toupin, D. Belanger, I. Hill, D. Quinn, J. Power Sources 140 (2005) 203.
[34] A. Alonso, V. Ruiz, C. Blanco, R. Santamaria, M. Granda, R. Menendez, S.G.E. Jager, Carbon 44 (2006) 441.
[35] T.E. Rufford, D. Hulicova-Jurcakova, Z. Zhu, G.Q. Lu, Electrochem. Commun. 10 (2008) 1594.
[36] M. Endo, Y.J. Kim, T. Takeda, T. Maeda, T. Hayashi, K. Koshiba, H. Hara, M.S. Dresselhaus, J. Electrochem. Soc. 148 (2001) A1135.
[37] E. Raymundo-Pinero, F. Leroux, F. Beguin, Adv. Mater. 18 (2006) 18772.
[38] E. Ito, S. Mozia, M. Okuda, T. Nakano, M. Toyoda, M. Inagaki, New Carbon Mater. 22 (2007) 321.
[39] E. Ito, H. Nakamura, M. Inagaki, TANSO No. 231 (2008) 8.
[40] Y. Kim, Y. Horie, Y. Matsuzawa, S. Ozaki, M. Endo, M. Dresselhaus, Carbon 42 (2004) 2423.
[41] S. Shiraishi, H. Kurihara, A. Oya, Carbon Sci. 1 (2001) 133.
[42] S. Shiraishi, H. Kurihara, L. Shi, T. Nakayama, A. Oya, J. Electrochem. Soc. 149 (2002) A855.
[43] Y. Kim, Y. Abe, T. Yanagiura, K. Park, M. Shimizu, T. Iwazaki, S. Nakagawa, M. Endo, M.S. Dresselhaus, Carbon 45 (2007) 2116.
[44] H. Nakagawa, A. Shudo, K. Miura, J. Electrochem. Soc. 147 (2000) 38.
[45] E. Frackowiak, K. Metenier, V. Bertagna, F. Beguin, Appl. Phys. Lett. 77 (2000) 2421.
[46] A. Oya, N. Kasahara, Carbon 38 (2000) 1141.
[47] Q. Jiang, M.Z. Qu, G.M. Zhou, B.L. Zhang, Z.L. Yu, Mater. Lett. 57 (2002) 988.
[48] M. Hahn, M. Baertschi, O. Barbieri, J.-C. Sauter, R. Koewtz, R. Gallay, Electrochem. Solid-State Lett. 7 (2004) A33.
[49] S. Yoon, S. Lim, Y. Song, Y. Ota, W. Qiao, A. Tanaka, I. Mochida, Carbon 42 (2004) 1723.
[50] S. Shiraishi, M. Kibe, T. Yokoyama, H. Kurihara, N. Patel, A. Oya, Y. Kaburagi, Y. Hishiyama, Appl. Phys. A 82 (2006) 585.
[51] B. Xu, F. Wu, R. Chen, G. Cao, S. Chen, G. Wang, Y. Yang, J. Power Sources 158 (2006) 773.
[52] K. Jurewicz, K. Babel, R. Pietrzak, S. Delpeux, H. Wachowska, Carbon 44 (2006) 2368.
[53] S. Shiraishi, T. Miyauchi, R. Sasaki, N. Nishina, A. Oya, R. Hagiwara, Electrochemistry 75 (2007) 619.
[54] J.F. Snyder, E.L. Wong, C.W. Hubbard, J. Electrochem. Soc. 156 (2009) A215.
[55] M. Toyoda, M. Inagaki, J. Phys. Chem. Solids 65 (2004) 109.
[56] M. Toyoda, Y. Tani, Y. Soneda, Carbon 42 (2004) 2833.
[57] Y. Soneda, M. Toyoda, K. Hashiya, J. Yamashita, M. Kodama, H. Hatori, M. Inagaki, Carbon 41 (2003) 2680.
[58] Y. Soneda, J. Yamashita, M. Kodama, H. Hatori, M. Toyoda, M. Inagaki, Appl. Phys. A 82 (2006) 575.
[59] T. Kyotani, T. Nagai, S. Inoue, A. Tomita, Chem. Mater. 9 (1997) 609.
[60] K. Matsuoka, Y. Yamagishi, T. Yamazaki, N. Setoyama, A. Tomita, T. Kyotani, Carbon 43 (2005) 876.
[61] P.X. Hou, T. Yamazaki, H. Orikasa, T. Kyotani, Carbon 43 (2005) 2624.
[62] H. Nishihara, H. Itoi, T. Kogure, P. Hou, H. Touhara, F. Okino, T. Kyotani, Chem. Eur. J. 15 (2009) 5355.
[63] C. Portet, Z. Yang, Y. Korenblit, Y. Gogotsi, R. Mokaya, G. Yushin, J. Electrochem. Soc. 156 (2009) A1.
[64] H. Wang, Q. Gao, J. Hu, Z. Chen, Carbon 47 (2009) 2259.
[65] R. Ryoo, S.H. Joo, S. Jun, J. Phys. Chem. B 103 (1999) 7743.
[66] J. Lee, S. Yoon, T. Hyeon, S.M. Oh, K.B. Kim, Chem. Commun. (1999) 2177.
[67] J. Lee, J. Kim, T. Hyeon, Adv. Mater. 18 (2006) 2073.
[68] A.B. Fuertes, F. Pico, J.M. Rojo, J. Power Sources 133 (2004) 329.
[69] A.B. Fuertes, G. Lota, T.A. Centeno, E. Frackowiak, Electrochim. Acta 50 (2005) 2799.
[70] K. Jurewicz, C. Vix-Guterl, E. Frackowiak, S. Saadallah, M. Reda, J. Parmentier, J. Patrin, F. Beguin, J. Phys. Chem. Solids 65 (2004) 287.
[71] C. Vix-Guterl, E. Frackowiak, K. Jurewicz, M. Friebe, J. Parmentier, F. Beguin, Carbon 43 (2005) 1293.
[72] W. Xing, S.Z. Qiao, R.G. Ding, F. Li, G.Q. Lu, Z.F. Yan, H.M. Cheng, Carbon 44 (2006) 216.
[73] M. Sevilla, S. Alvarez, T.A. Centeno, A.B. Fuertes, F. Stoeckli, Electrochim. Acta 52 (2007) 3207.
[74] T.A. Centeno, M. Sevilla, A.B. Fuertes, F. Stoeckli, Carbon 43 (2005) 3012.
[75] J. Gorka, A. Zawislak, J. Choma, M. Jaroniec, Carbon 46 (2008) 1159.
[76] K. Xia, Q. Gao, J. Jiang, J. Hu, Carbon 46 (2008) 1718.
[77] T. Morishita, Y. Soneda, T. Tsumura, M. Inagaki, Carbon 44 (2006) 2360.
[78] T. Morishita, L. Wang, T. Tsumura, M. Toyoda, H. Konno, M. Inagaki, TANSO No. 242 (2010) 60.

[79] T. Morishita, T. Tsumura, M. Toyoda, J. Przepiórski, A.W. Morawski, H. Konno, M. Inagaki, Carbon 48 (2010) 2690.
[80] J.A. Fernandez, T. Morishita, M. Toyoda, M. Inagaki, F. Stoeckli, T.A. Centeno, J. Power Sources 175 (2008) 675.
[81] D.W. Wang, F. Li, M. Liu, G.Q. Lu, H.M. Cheng, Angew. Chem. Int. Ed. 47 (2008) 373.
[82] S. Shiraishi, H. Kurihara, H. Tsubota, A. Oya, Y. Soneda, Y. Yamada, Electrochem. Solid-State Lett. 4 (2001) A5.
[83] S. Shiraishi, Y. Aoyama, H. Kurihara, A. Oya, Y. Yamada, Mol. Cryst. Liquid Cryst. 388 (2002) 129.
[84] Y. Yamada, O. Tanaike, T.-T. Liang, H. Hatori, S. Shiraishi, A. Oya, Electrochem. Solid-State Lett. 5 (2002) A283.
[85] Y. Gogotsi, A. Nikitin, H. Ye, W. Zou, J.E. Fischer, B. Yi, H.C. Foley, M.W. Barsoum, Nature Mater. 2 (2003) 591.
[86] Y. Gogotsi, R.K. Dash, G. Yushin, T. Yildirim, G. Laudisio, J.E. Fischer, J. Am. Chem. Soc. 127 (2005) 16006.
[87] R.K. Dash, G. Yushin, Y. Gogotsi, Micropor. Mesopor. Mater. 86 (2005) 50.
[88] J. Chmiola, G. Yushin, R. Dash, Y. Gogotsi, J. Power Sources 158 (2006) 765.
[89] A. Jänes, L. Permann, M. Arulepp, E. Lust, Electrochem. Commun. 5 (2004) 313.
[90] J. Chmiola, G. Yushin, Y. Gogotsi, C. Porter, P. Simon, P.L. Taberna, Science 313 (2006) 1760.
[91] R. Lin, P.I. Taberna, J. Chmioda, D. Guay, Y. Gogotsi, P. Simon, J. Electrochem. Soc. 156 (2009) A7.
[92] J. Chmiola, G. Yushin, R.K. Dash, E.N. Hoffman, J.E. Fischer, M.W. Barsoum, Y. Gogotsi, Electrochem. Solid-State Lett. 8 (2005) A357.
[93] H. Wang, Q. Gao, Carbon 47 (2009) 820.
[94] R. Salinger, U. Fischer, C. Herta, J. Fricke, J. Non-Cryst. Solids 225 (1998) 81.
[95] Y. Tao, M. Endo, K. Kaneko. Recent Patents Chem. Eng. 1 (2009) 192.
[96] B. Fang, Y.-Z. Wei, K. Maruyama, M. Kumagai, J. Appl. Electrochem. 35 (2005) 229.
[97] C. Lin, J.A. Ritter, B.N. Popov, J. Electrochem. Soc. 146 (1999) 3639.
[98] Y. Kuwahara, H. Yano, Y. Kanematsu, H. Oda, TANSO No. 235 (2008) 263.
[99] C. Liu, A.J. Bard, F. Wudl, I. Weitz, J.R. Heath, Electrochem Solid-State Lett. 2 (1999) 577.
[100] S. Shiraishi, H. Kurihara, K. Okabe, D. Hulicova, A. Oya, Electrochem. Commun. 4 (2002) 593.
[101] E. Frackowiak, K. Jurewicz, S. Delpeux, F. Beguin, J. Power Sources 97/98 (2001) 822.
[102] K.A. An, W.S. Kim, Y.S. Park, Y.C. Choi, S.M. Lee, D.C. Chung, D.J. Bae, S.C. Lim, Y.H. Lee, Adv. Mater. 13 (2001) 497.
[103] G.C. Liu, H.T. Fang, F. Li, M. Liu, H.M. Cheng, J. Power Sources 160 (2006) 758.
[104] K. Hata, D.N. Futaba, K. Mizuno, T. Namai, M. Yumura, S. Iijima, Science 306 (2004) 1362.
[105] O. Tanaike, D.N. Futaba, K. Hata, H. Hatori, Carbon Lett. 10 (2009) 90.
[106] O. Kimizuka, O. Tanaike, J. Yamashita, T. Hiraoka, D.N. Futaba, K. Hata, K. Machida, S. Suematsu, K. Tamamitsu, S. Saeki, Y. Yamada, H. Hatori, Carbon 46 (2008) 1999.
[107] T. Hiraoka, A.I. Najafabadi, T. Yamada, D.N. Futaba, S. Yasuda, O. Tanaike, H. Hatori, M. Yumura, S. Iijima, K. Hata, Adv. Funct. Mater. 20 (2009) 422.
[108] D.N. Futaba, K. Hata, T. Yamada, T. Hiraoka, Y. Hayamizu, Y. Kakudate, O. Tanaike, H. Hatori, M. Yumura, S. Iijima, Nature Mater. 5 (2006) 987.
[109] Y. Yamada, O. Kimizuka, O. Tanaike, K. Machida, S. Suematsu, K. Tamamitsu, S. Saeki, Y. Yamada, H. Hatori, Electrochem. Solid-State Lett. 12 (2009) K14.
[110] C. Niu, E.K. Sichel, R. Hoch, D. Moy, H. Tennent, Appl. Phys. Lett. 70 (1997) 1480.
[111] R.Z. Ma, J. Liang, B.Q. Wei, B. Zhang, C.L. Xu, D.H. Wu, J. Power Sources 84 (1999) 126.
[112] C. Emmenegger, P. Mauron, P. Sudan, P. Wenger, V. Hermann, R. Gallay, A. Züttel, J. Power Sources 124 (2003) 321.
[113] Y. Honda, T. Haramoto, M. Takeshige, H. Shiozaki, T. Kitamura, M. Ishikawa, Electrochem. Solid State Lett. 10 (2007) A106.
[114] Y. Honda, M. Takeshige, H. Shiozaki, T. Kitamura, K. Yoshikawa, S. Chakarabarti, O. Suekane, L. Pan, Y. Nakayama, M. Yamagata, M. Ishikawa, J. Power Sources 185 (2008) 1580.
[115] W. Lu, L. Qu, K. Henry, L. Dai, J. Power Sources 189 (2009) 1270.
[116] B.E. Conway, V. Birss, J. Wojtowicz, J. Power Sources 66 (1997) 1.
[117] D. Qu, J. Power Sources 109 (2002) 403.
[118] M.J. Bleda-Martinez, J.A. Macia-Agullo, D. Lozano-Castello, E. Morallon, D. Cazorla-Amoros, A. Linares-Solano, Carbon 43 (2005) 2677.
[119] V. Ruiz, C. Blanco, E. Raymundo-Pinero, V. Kohmenko, F. Beguin, R. Santamaria, Electrochim. Acta 52 (2007) 4969.
[120] C. Hsieh, H. Teng, Carbon 40 (2002) 667.
[121] K. Okajima, K. Ohta, M. Sudoh, Electrochim. Acta 50 (2005) 2227.
[122] Y.R. Nian, H. Teng, J. Electrochem. Soc. 149 (2002) A1008.
[123] H. Oda, A. Yamashita, S. Minoura, M. Okamoto, T. Morimoto, J. Power Sources 158 (2006) 1510.
[124] C. Hu, C. Wang, J. Power Sources 125 (2004) 299.
[125] Y. Nian, H. Teng, J. Electroanal. Chem. 540 (2003) 1197.
[126] M. Kodama, J. Yamashita, Y. Soneda, H. Hatori, K. Kamegawa, Carbon 45 (2007) 1105.
[127] K. Jurewicz, R. Pietrzak, P. Nowicki, H. Wachowska, Electrochim. Acta 53 (2008) 5469.
[128] D. Hulicova, M. Kodama, H. Hatori, Chem. Mater. 18 (2006) 2318.
[129] Z.H. Zhu, H. Hatori, S.B. Wang, G.Q. Lu, J. Phys. Chem. B 109 (2005) 167449.
[130] D. Hulicova, J. Yamashita, Y. Soneda, H. Hatori, M. Kodama, Chem. Mater. 17 (2005) 1241.
[131] Y. Yamada, O. Tanaike, S. Shiraishi, TANSO No. 215 (2004) 285.
[132] K. Jurewicz, K. Babel, A. Ziolkowski, H. Wachowska, M. Kozlowski, Fuel Process. Technol. 77/78 (2002) 191.
[133] K. Jurewicz, K. Babel, A. Ziolkowski, H. Wachowska, Electrochim. Acta 48 (2003) 1491.
[134] K. Jurewicz, K. Babel, A. Zioekowski, H. Wachowska, J. Phys. Chem. Solids 65 (2004) 269.
[135] M. Kodama, J. Yamashita, Y. Soneda, H. Hatori, S. Nishimura, K. Kamegawa, Mater. Sci. Eng. B 108 (2004) 156.
[136] S. Shiraishi, H. Mamyouda, TANSO No. 232 (2008) 61.
[137] G. Lota, B. Grzyb, H. Machnikowaka, J. Machnikowaki, E. Frackowiak, Chem. Phys. Lett. 404 (2005) 53.
[138] M. Kodama, J. Yamashita, Y. Soneda, H. Hatori, K. Kamegawa, I. Moriguchi, Chem. Lett. 35 (2006) 680.
[139] W. Li, D. Chen, Z. Li, Y. Shi, Y. Wang, J. Huang, D. Zhao, Z. Jiang, Electrochim. Commun. 9 (2007) 569.
[140] H. Konno, H. Onishi, N. Yoshizawa, K. Azumi, J. Power Sources 195 (2010) 667.
[141] M. Seredych, D. Hulicova-Jurcakova, G.Q. Lu, T.J. Bandosz, Carbon 46 (2008) 1475.
[142] E. Frackowiak, G. Lota, J. Machnikowski, C. Vix-Gutrl, F. Beguin, Electrochim. Acta 51 (2006) 2209.
[143] D.-W. Wang, F. Li, Z.-G. Chen, G.Q. Lu, H.-M. Cheng, Chem. Mater. 20 (2008) 7195.
[144] T. Ito, M. Ushiro, K. Fushimi, K. Azumi, H. Konno, TANSO No. 239 (2009) 156.
[145] H. Guo, Q. Gao, J. Power Sources 186 (2009) 551.
[146] H. Konno, T. Ito, M. Ushiro, K. Fushimi, K. Azumi, J. Power Sources 195 (2010) 1739.
[147] S. Sepehri, B.B. Garcia, Q. Zhang, G. Cao, Carbon 47 (2009) 1436.
[148] J.P. Zheng, P.J. Cygan, T.R. Jow, J. Electrochem. Soc. 142 (1995) 2699.
[149] .H. Chang, C.C. Hu, Electrochem. Solid-State Lett. 7 (2004) A466.
[150] P. Soudan, J. Gaudet, D. Guay, D. B'Elanger, R. Schulz, Chem. Mater. 14 (2002) 1210.
[151] J.M. Miller, B. Dunn, T.D. Tran, R.W. Pekala, J. Electrochem. Soc. 144 (1997) L309.
[152] Y. Sato, K. Yomogida, T. Nanaumi, K. Kobayakawa, Y. Ohsawa, M. Kawai, Electrochem. Solid-State Lett. 3 (2000) 113.
[153] M. Ramani, B.S. Haran, R.E. White, B.N. Popov, L. Arsov, J. Power Sources 93 (2001) 209.
[154] H. Kim, B.N. Popov, J. Power Sources 104 (2002) 52.
[155] Y. Takasu, T. Nakamura, Y. Murakami, Chem. Lett. (1998) 1215.
[156] Y. Takasu, T. Ohnuma, W. Sugimoto, Y. Murakami, Electrochemistry 67 (1999) 1187.
[157] N.L. Wu, S.Y. Wang, C.Y. Han, D.S. Wu, L.R. Shiue, J. Power Sources 113 (2003) 173.
[158] M. Ushiro, A. Yoneda, N. Iwasa, K. Fushimi, H. Konno, TANSO No. 238 (2009) 121.
[159] T. Morishita, Y. Soneda, H. Hatori, M. Inagaki, Electrochim. Acta 52 (2007) 2478.
[160] L. Wang, T. Morishita, M. Toyoda, M. Inagaki, Electrochim. Acta 53 (2007) 882.
[161] L. Wang, M. Toyoda, M. Inagaki, Adv. Sci. Technol. 46 (2008) 491.
[162] V. Ruiz, C. Blanco, M. Granda, R. Santamarfa, Electrochim. Acta 54 (2008) 305.
[163] A. Yoshino, T. Tsubata, M. Shimoyamada, H. Satake, Y. Okano, S. Mori, S. Yata, J. Electrochem. Soc. 151 (2004) A2180.
[164] T. Aida, K. Yamada, M. Morita, Electrochem. Solid-State Lett. 9 (2006) A534.
[165] T. Aida, I. Murayama, K. Yamada, M. Morita, J. Power Sources 166 (2007) 462.
[166] M.S. Hong, S.H. Lee, S.W. Kim, Electrochem. Solid-State Lett. 5 (2002) A227.
[167] T. Brousse, M. Toupin, D. B'Elanger, J. Electrochem. Soc. 151 (2004) A614–A622.
[168] T. Brousse, P.L. Taberna, O. Corsnier, R. Dugas, P. Guillemer, Y. Scudeller, Y. Zhou, F. Favier, D. Belanger, P. Simon, J. Power Sources 173 (2007) 633.
[169] V. Khomenko, E. Raymundo-Pinero, F. Beguin, J. Power Sources 153 (2006) 183.
[170] C. Xu, B. Li, H. Du, F. Kang, Y. Zeng, J. Power Sources 180 (2008) 664.
[171] C. Xu, H. Du, B. Li, F. Kang, Y. Zeng, J. Electrochem. Soc. 156 (2009) A73.
[172] C. Xu, H. Du, B. Li, F. Kang, Y. Zeng, J. Electrochem. Soc. 156 (2009) A435.
[173] D.W. Wang, F. Li, H.M. Cheng, J. Power Sources 185 (2008) 1563.
[174] A. Laforgue, P. Simon, J.F. Fauvarque, J.F. Sarrau, P. Lailler, J. Electrochem. Soc. 148 (2001) A1130.
[175] A. Lafogue, P. Simon, J.F. Fauvarque, M. Mastragostino, F. Soavi, J.F. Sarrau, P. Lailler, M. Conte, E. Rossi, S. Saguatti, J. Electrochem. Soc. 150 (2003) A645.
[176] C. Arbizzani, S. Beninati, M. Lazzari, F. Soavi, M. Mastragostino, J. Power Sources 174 (2007) 648.
[177] K. Machida, S. Suematsu, S. Ishimoto, K. Tamamitsu, J. Electrochem. Soc. 155 (2008) A970.
[178] .G. Amatucci, F. Badway, A.D. Pasquier, T. Zheng, J. Electrochem. Soc. 148 (2001) A930.
[179] A.D. Pasquier, I. Plitz, J. Gural, S. Menocal, G.G. Amatucci, J. Power Sources 113 (2003) 62.
[180] A.D. Pasquier, I. Plitz, S. Menocal, G.G. Amatucci, J. Power Sources 115 (2003) 171.
[181] L. Wang, M. Toyoda, M. Inagaki, New Carbon Mater. 23 (2008) 1115.
[182] L. Wang, M. Inagaki, M. Toyoda, TANSO No. 240 (2009) 230.

[183] G. Gryglewicz, J. Machnikowski, E. Lorenc-Grabowska, G. Lota, E. Frackowiak, Electrochim. Acta 50 (2005) 1197.
[184] Y. Wen, G. Cao, J. Cheng, Y. Yang, J. Electrochem. Soc. 152 (2005) A1770.
[185] L. Wang, M. Fujita, M. Inagaki, Electrochim. Acta 51 (2006) 4096.
[186] D. Aurbach, M.D. Levi, G. Salitra, N. Levy, E. Pollak, J. Muthu, J. Electrochem. Soc. 155 (2008) A745.
[187] D.-W. Wang, F. Li, M. Liu, G.Q. Lu, H.-M. Cheng, J. Phys. Chem. C 112 (2008) 9950.
[188] T.A. Centeno, F. Stoeckli, Electrochim. Acta 52 (2006) 560.